LAWRENCE
LIVERMORE
NATIONAL
LABORATORY

LLNL-JRNL-772309

Control of Physical and Chemical Processes with Metamaterials and Metallic Surfaces

V. N. Peters, S. R. Prayakarao, S. R. Koutsares, C. E. Bonner , M. A. Noginov

April 17, 2019

ACS Photonics

Disclaimer

This document was prepared as an account of work sponsored by an agency of the United States government. Neither the United States government nor Lawrence Livermore National Security, LLC, nor any of their employees makes any warranty, expressed or implied, or assumes any legal liability or responsibility for the accuracy, completeness, or usefulness of any information, apparatus, product, or process disclosed, or represents that its use would not infringe privately owned rights. Reference herein to any specific commercial product, process, or service by trade name, trademark, manufacturer, or otherwise does not necessarily constitute or imply its endorsement, recommendation, or favoring by the United States government or Lawrence Livermore National Security, LLC. The views and opinions of authors expressed herein do not necessarily state or reflect those of the United States government or Lawrence Livermore National Security, LLC, and shall not be used for advertising or product endorsement purposes.

Control of Physical and Chemical Processes with Nonlocal Metal-Dielectric Environments

Vanessa N. Peters[1,2*], Srujana Prayakarao[1,3*], Samantha R. Koutsares[1], Carl. E. Bonner[1], Mikhail A. Noginov[1*]

[1] *Center for Materials Research, Norfolk State University, Norfolk, VA 23504*
[2] *Currently with Lawrence Livermore National Laboratory, Livermore, CA 94550*
[3] *Currently with University of Kansas, Lawrence, KS 66045*
*mnoginov@nsu.edu

* These two authors contributed to the work equally

Abstract

In this *Perspective*, we make the case that (meta) material platforms that were originally designed to control propagation of light, can affect scores of physical and chemical phenomena, which are often thought to lie outside of the traditional electrodynamics domain. We show that nonlocal metal-dielectric environments, which can be as simple as metal-dielectric interfaces, can control spontaneous and stimulated emission, Förster energy transfer, wetting contact angle, and rates of chemical reactions. The affected phenomena can occur in both strong and weak coupling regimes and the large coupling strength seems to enhance the effects of non-local environments. This intriguing field of study has experienced a rapid growth over the last decade and many exciting discoveries and applications are expected in the years to come.

Keywords: metamaterials, plasmonics, nonlocal metal-dielectric environment, weak and strong coupling regimes.

PART I. INTRODUCTION AND REVIEW OF FUNDAMENTAL CONCEPTS

Manipulation of light with dielectric media and metallic surfaces is not limited to traditional large-scale optics, like eyeglass lenses and looking glasses. Thus, metal-dielectric interfaces and metallic nanostructures support a variety of propagating and localized surface plasmons (SPs) – resonant oscillations of free electron density coupled to electromagnetic waves. Surface plasmons can confine and strengthen electric and magnetic fields oscillating at optical frequencies and enhance spontaneous emission and Raman scattering [1],[2]. On the other hand, last two decades witnessed rapid development of metamaterials – engineered materials comprised of sub-wavelength inclusions with rationally designed shapes, sizes, compositions and mutual orientations (commonly) embedded in a dielectric matrix [3],[4],[5]. Nearly fantastic theoretical predictions and experimental demonstrations of metamaterials range from negative index of refraction to invisibility optical cloaking. Metamaterials can govern the rate [6,7,8,9,10,11,12,13,14], the spectrum [15] and the directionality [10,16] of spontaneous emission. More recently, it has been shown that metamaterials and, more generally, a variety of nanoscopic metal-dielectric structures can control scores of physical phenomena, including Förster energy transfer [17,18,19], van der Waals forces [20,21] and chemical reactions [22,23,24,25,26], which lie outside of a traditional electrodynamics domain. The phenomena above are of particular interest to the present discussion.

This *Perspective* is organized as follows. In Part I, following Introduction, we briefly review several Fundamental Concepts, including spontaneous emission, energy transfer, light-matter interactions (in weak and strong coupling regimes), van der Waals forces, and rates of chemical reactions. These processes are discussed in more detail in Part II, which includes (i) Control of Emission with Hyperbolic Metamaterials, (ii) Control of Energy Transfer with Nonlocal Metal-Dielectric Environments, (iii) Long-Range Wetting Transparency on Top of Layered Metal-Dielectric Substrates, and (iv) Control of Chemical Reactions in Weak and Strong Coupling Regimes. These phenomena are unified by underlying concept of controlling material's polarizability and dipole-dipole interactions with inhomogeneous metal/dielectric environments. The major results and conclusions are summarized in Part III (Summary).

Fundamental Concepts

Control of Spontaneous Emission with Electromagnetic Environments Spontaneous emission is one of the most fundamental phenomena in physics and optics. Following the Fermi's Golden Rule, [27], its rate is proportional to the density of final states – the number of modes per frequency interval $d\omega$ and per volume (known as Photonic Density of States, PDOS, or Local Density of states, LDOS), which is given by [28]

$$p(\omega)d\omega = \omega^2 n^3 / (\pi^2 c^3) d\omega . \quad (1)$$

Here ω is angular frequency, n is the refractive index and c is the speed of light. It has been predicted by Purcell [29] that the rate of spontaneous emission, which, otherwise is low, can be increased by orders of magnitude if the emitter is placed in a cavity with a large quality factor Q. The corresponding spontaneous emission enhancement factor (known as the Purcell factor) is equal to

$$f = 3Q\lambda^3 / 4\pi^2 V , \quad (2)$$

where λ is the wavelength and V is the volume of the cavity [29].

Three decades later, Drexhage et al. have demonstrated [30,31] that spontaneous emission rate of an emitter (in the optical range) varies with the distance to a metallic mirror, following nodes and anti-nodes of a standing wave formed by a superposition of the incident and reflected light waves and the corresponding minima and maxima in the spatial distribution of PDOS, Fig. 1. Photonic density of states and the rates of spontaneous emission can be strongly modified by high-Q resonators [32,33], photonic band crystals [34,35,36,37], plasmonic structures [38,39,40], and other photonic environments. However, in many cases, the singularity of PDOS is spectrally narrow, which limits its effect on a broad-band spontaneous emission.

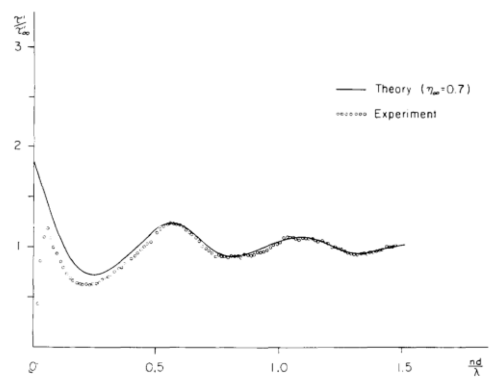

Fig. 1. Fluorescence decay time of Eu^{3+} in front of silver mirror; solid line – calculation done at the quantum yield η_∞=0.7, circles – experiment. Adopted from Ref. [30].

The Renaissance in control of spontaneous emission with engineered photonic environments followed emergence of metamaterials with hyperbolic dispersion – artificial nanostructured materials, whose dielectric permittivities in orthogonal directions have opposite signs [41,42,43,44,45,46,47] resulting in hyperbolic isofrequency dispersion curves for extraordinary waves and broadband singularity of PDOS [10,12,48].

The isofrequency dispersion surface, for extraordinary waves, in a (loss-less) uniaxial hyperbolic metamaterial, is given by

$$\frac{k_x^2 + k_y^2}{\varepsilon_{zz}} + \frac{k_z^2}{\varepsilon_{xx}} = \left(\frac{\omega}{c}\right)^2 , \quad (3)$$

where $\varepsilon_x=\varepsilon_y$ and ε_z are the dielectric permittivities in x, y and z directions, and $k_{x,y,z}$ are the wavevector components. The shapes of the dispersion surfaces for ($\varepsilon_x=\varepsilon_y>0$ and $\varepsilon_z<0$) and ($\varepsilon_x=\varepsilon_y<0$ and $\varepsilon_z>0$) are depicted in Figs. 2a and 2b, respectively.

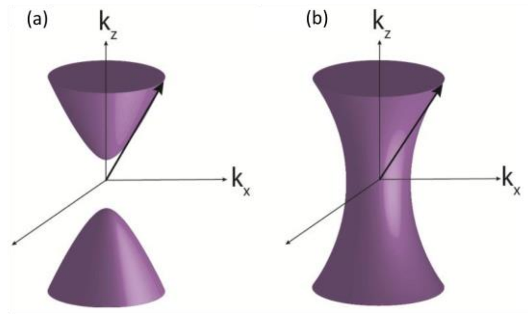

Fig. 2. Hyperboloid isofrequency dispersion surfaces for (a) $\varepsilon_x=\varepsilon_y>0$ and $\varepsilon_z<0$ and (b) $\varepsilon_x=\varepsilon_y<0$ and $\varepsilon_z>0$). Adopted from Ref. [47].

Experimentally, enhancement of the rate of spontaneous emission with hyperbolic metamaterials was first demonstrated in Ref. [6], followed by scores of related works exploring different morphologies and emitters [7,8,9,10,11,12,13,14]. These studies are discussed in Part II below.

Förster Energy Transfer Excited molecule can make a transition to a ground state by emitting a photon, as in the case of spontaneous emission [28]. Among many other ways of giving away its energy (*e.g.* to molecular vibrations [49], phonons [50], plasmons [51,52], polaritons [53], etc.), it can transfer its excitation to a closely situated ground state molecule [54] – the process of particular interest in this study, Fig. 3. In general, if two molecules are coupled in some way (*e.g. via* Coulomb interactions), this can result in an energy transfer between them [54]. This energy transfer can be reversible (oscillatory), when the coupling strength Ω is much larger than (i) the decay rates (inverse *longitudinal* decay times) of both donor and acceptor ($1/\tau_d$ and $1/\tau_a$) and (ii) the rate of the phase correlation decay (inverse *transverse* relaxation time, $1/T_2$ [54]). In the latter case, the splitting of the energy eigenvalues of the interacting molecules is expected [54] (as discussed in Part II). Alternatively, the energy transfer can be irreversible, when $T_2 << \tau_d << \tau_a$ [54]. Following Ref. [54], the term *energy transfer* should be reserved only for those cases, which involve substantial irreversibility and a relaxation process (to the ground state). However, this terminology is not uniformly followed by all authors.

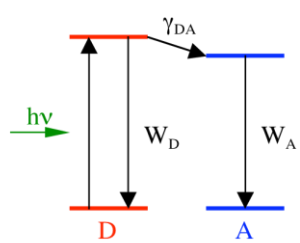

Fig. 3. Schematic of irreversible Förster donor-acceptor energy transfer showing absorption of light in donor, combination of radiative and non-radiative relaxation processes in donor (W_D), donor-acceptor energy transfer (γ_{DA}), and the relaxation processes in acceptor (W_A).

Förster developed the theory of energy transfer for molecules having broad spectra in a condensed medium [54,55,56,57]. The theory is based on the perturbation model in adiabatic approximation. The theory assumes that the energy transfer occurs owing to a dipole-dipole interaction between molecules, which is so weak that it does not change the energy eigenvalues of the molecules. Förster has shown that under such conditions, the probability of the energy transfer W can be expressed in terms of the integral of the overlap of the luminescence and absorption spectra of interacting molecules:

$$W = \frac{3}{2}\chi^2 \frac{R_0^6}{\tau_0 R^6}, \tag{4}$$

where

$$R_0^6 = \frac{3}{2(2\pi)^5}\frac{\eta_0}{n^4}\int F(\bar{\nu})\sigma(\bar{\nu})\frac{d\bar{\nu}}{\bar{\nu}^4}. \tag{5}$$

Here R is the distance between donor and acceptor, R_0 is the characteristic radius at which the transfer probability equals to the probability of spontaneous emission in the donor molecule, τ_0 is the experimental donor life-time, η_0 is the quantum yield of donor luminescence, χ is the factor taking into account relative orientations of the interacting dipoles (χ^2=2/3 if all the relative orientations are equally probable), F($\bar{\nu}$) is the normalized radiation spectrum, $\sigma(\bar{\nu})$ is the cross-section of acceptor absorption, $\bar{\nu}$ is the frequency in cm^{-1}, and n is the refractive index.

Förster was also the first to average the probability of transfer over molecules in a solid solution, resulting in emission kinetics $n(t)$, which can be compared with experimental data [54,55,56,57,]

$$n(t) = n_0 \exp\left(-t/\tau_0 - 2q\sqrt{t/\tau_0}\right), \tag{6}$$

where $q \approx 3.14 R_0^3 c_A$, n_0 is the initial concentration of excited donors (pumped with a short pulse), c_A is the concentration of acceptors, and t is time [54].

*van der Waals interactions and wetting* The concept of interaction between neutral atoms or molecules has been proposed by van der Waals in 1873 [58]. Subsequently, three different, although related, processes, which contribute to this phenomenon, have been identified as (1) interaction between randomly oriented permanent dipoles and molecules [59,60,61], (2) interaction between randomly oriented permanent dipoles and induced dipoles [62,63], and (3) interactions between fluctuating dipoles and induced dipole (dispersive or London mechanism [64]). In the latter case, fluctuation of dipole moments results from thermal or quantum effects. The dispersive mechanism is better studied in the literature and believed to be primarily responsible for interaction between various macroscopic bodies [65].

In Fig. 4a, fluctuating dipole in atom 1 induces dipole in atom 2 and these two dipoles attract each other. If two slabs are comprised of multiple dipoles, the slabs can be attracted to each other as well, Fig. 4b. The gap between the slabs can be filled with a medium M, Fig. 4b. This can change both the magnitude and the sign of the force exerted by slabs 1 and 2 on each other [66]. If an external body, such as metallic mirror, is brought to the vicinity of the two dipoles, it will produce virtual image dipoles and alter the net attractive force between atoms 1 and 2, Fig. 4c. Likewise, the external body 3 will change the interaction force between the two macroscopic slabs 1 and 2, Fig. 4d.

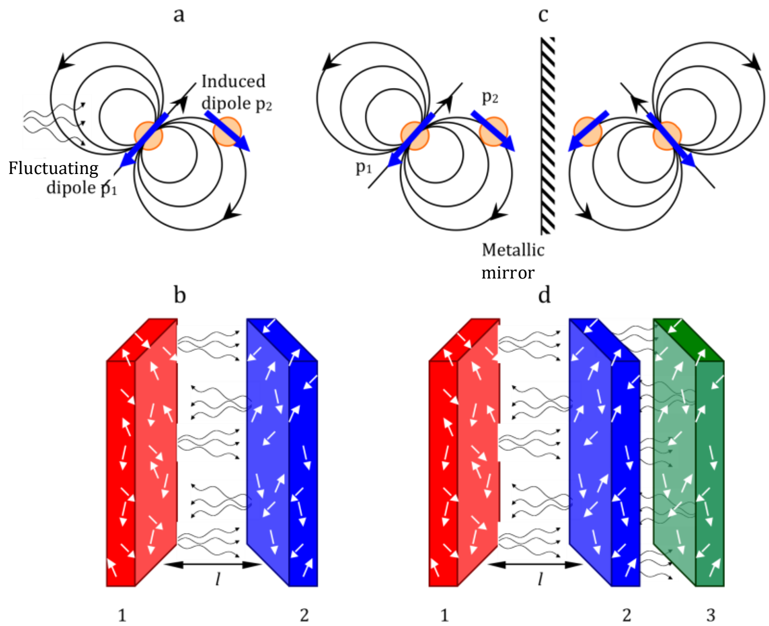

Fig. 4. (a) Interaction of fluctuating dipole p_1 and induced dipole p_2. (b) Interaction of two slabs 1 and 2, when the gap between the slabs is filled with the medium M [20]. (c) Same as in Fig. 4a in vicinity of the metallic mirror that produces image charges. (d) Same as in Fig. 4b in presence of slab 3 [21]. Adopted from Ref.[21].

It has been shown [66,67] that the force between two semi-infinite slabs 1 and 2 separated by the spacer M and the corresponding energy of interaction U depend on dielectric permittivities of all three media involved, $\varepsilon_1(\omega)$, $\varepsilon_2(\omega)$, $\varepsilon_M(\omega)$, integrated over the whole frequency range [21]. In the non-retarded regime, when the distance between the two slabs l is much smaller than the speed of light c divided by the maximal characteristic frequency $\omega_{UV}/2\pi$ (of e.g. ultraviolet absorption band) contributing to the interaction energy, the latter is equal to $U = \frac{A}{12\pi l^2}$. Here A, historically termed "Hamaker constant", is determined by dielectric permittivities or molecular polarizabilities of the interacting media [65,68,69]. In the simplest case of two identical dielectric slabs separated by vacuum, an approximate value of the Hamaker constant is given by the equation [69]

$$A \approx \frac{3}{16\sqrt{2}} \frac{\left(n_0^2 - 1\right)^2}{\left(n_0^2 + 1\right)^{3/2}} \mathrm{h}\omega_{UV}, \qquad (7)$$

where n_0 is the refractive index in the visible range. In the retarded (Casimir [67,68,69,70,71]) regime, $l \geq 2\pi c/\omega_{UV}$, the $\sim l^{-2}$ dependence changes to the $\sim l^{-3}$ dependence [65,66,67,68,69,70,71]. Correspondingly, van der Waals forces can be viewed as Casimir forces in the electrostatic limit.

Note that the $\sim l^{-2}$ dependence of the interaction energy has a substantially longer range than the $\sim l^{-6}$ dependence for interacting molecular dipoles. This is the important result of Hamaker, who has shown that although the range of atomic forces is of the order of atomic dimensions, the sum of the dispersion energies leads to interaction of nanoscopic colloidal bodies at the characteristic distances comparable to their dimensions [68,72].

The considerations above apply to both solids and liquids [21]. Correspondingly, one can calculate the free energy change due to cohesion of the material ΔU [65], which is related to the surface tension ©$=\Delta U/2$, *e.g.*

of a droplet of liquid in vacuum. If the droplet resides on a solid surface, then, in a similar way, one can introduce the free energy and the surface tension for the liquid-solid interface, ©$_{ls}$, liquid-vapor interface, ©$_{lv}$, and solid-liquid interface, ©$_{sv}$. They collectively determine the wetting angle θ, defined as shown in Fig. 5 a,b,

$$\cos\theta = (\gamma_{sv} - \gamma_{sl}) / \gamma_{lv} \tag{8}$$

(Young equation [69,73]). The third body brought to the vicinity of slabs 1 and 2 can change the interaction energy between them, Fig. 4d. Correspondingly, the wetting angle, which can be measured experimentally, should be sensitive to a change of the (non-local) dielectric environment in the vicinity of the solid-liquid interface. The experimental observation of this phenomenon is discussed in Part II below.

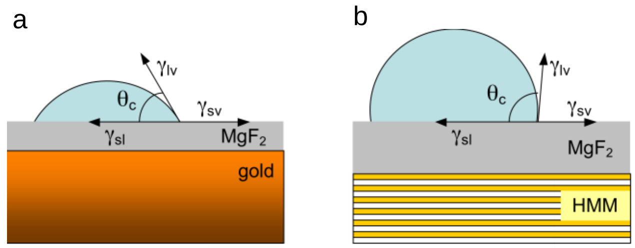

Fig. 5. Wetting angle for a droplet of water on top of MgF_2 layer with gold (a) and lamellar metamaterial (b) underneath. Adopted from Ref. [21].

Light-matter interactions in weak and strong coupling regimes As discussed above, the vicinity to plasmonic structures, lamellar metal/dielectric metamaterials and simple metallic surfaces can control scores of physical phenomena, including spontaneous emission [6,7,8,9,10,11,12,13,14,15], Förster energy transfer [17,18,19], van der Waals interactions [20,21], and chemical reactions [22,23,24,25,26] (below). Many of these processes occur in the regime of weak light-matter interaction, which affects transitions' rates but not the energy eigenvalues of interacting systems.

Even stronger effects can be observed at *strong coupling* between *e.g*. ensembles of dye molecules and resonant plasmonic structures or cavities [74,75,76]. In the latter regime, the rate of bidirectional energy exchange between two interacting oscillators is higher than the rates of relaxation and de-phasing [54], causing (i) formation of two hybrid energy states – upper and lower polariton branches – whose eigen-energies, separated by the Rabi frequency, are different from those of interacting constituents (Fig. 6a [77]) and (ii) an avoided crossing behavior of the corresponding dispersion curves (Fig. 6b).
There are two criteria of strong coupling used in the literature. According to one of them, strong coupling occurs when the Rabi splitting exceeds the spectral widths of the upper and the lower polariton branches. In this case, the coupling and the Rabi splitting can be small, ≤10 meV [78], but still exceed an even smaller widths of the spectral lines. According to the second criterion, the (ultra) strong coupling occurs when the value of the Rabi spitting, [22,23,75,79,80] is getting comparable with eigen-energies of non-interacting constituents [22]. This is the regime of coupling between cavities or plasmonic systems interacting with large ensembles of highly concentrated dye molecules. The record-high Rabi splitting of ~1.12 eV has been experimentally demonstrated in organic semiconductors coupled to cavity modes [81]. The latter coupling regime is of particular interest to the discussion below.

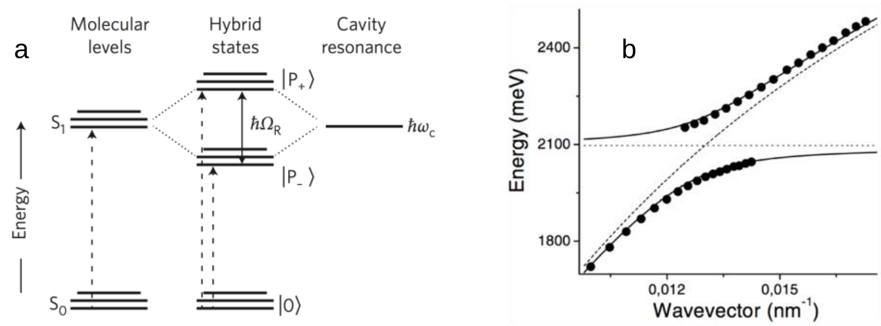

Fig. 6. (a) Rabi splitting in a resonant cavity. Interaction of a HOMO–LUMO (S_0–S_1) transition of a molecule resonant with a cavity mode $\hbar\omega_c$. Strong coupling leads to the formation of two hybrid light–matter (polaritonic) states (P^+ and P^-) separated by the Rabi splitting energy ($\hbar\Omega_R$). 0 represents the ground state. Adopted from [77]. (b) Strong coupling between an SPP mode (diagonal dotted line) and an excitonic mode (horizontal dashed line) [75]. The system is a metal film (that supports the SPP mode) coated with a polymeric film doped with aggregated dye molecules. The solid lines and circles show how these modes interact to produce an avoided crossing [79,75], the dashed lines show the dispersion expected in the absence of strong coupling . Adopted from [75].

Marcus theory and its extension to inhomogeneous dielectric environments As it was shown by Marcus [82,83,84,85,] dielectric environments can affect not only physical processes, but also chemical reactions. In simple terms, two reactants, donor and acceptor, have certain spatial distribution of electrical charges, which is balanced by an appropriate polarization of surrounding solvent molecules [24]. Transfer of an electron from donor to acceptor changes the local charge distribution and causes repolarization of solvent molecules. This change of polarization requires a so-called reorganization energy λ. It contributes to the strength of the potential barrier ΔG^*, which the reaction should overcome as it moves along the path from the reactants valley to the products valley, Fig. 7 [84].

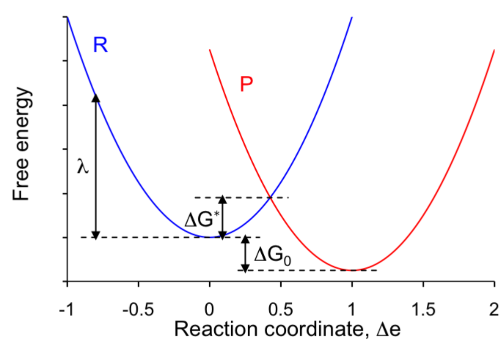

Fig. 7. Free energies of reactants R and products P (plus environments) plotted vs. reaction coordinate Δe. (Adopted from [24]). In the "normal region" regime, depicted in the figure, the R and P curves intersect on the right of the minimum of R. Whereas in the "inverted region" regime, the same two curves intersect on the left of the minimum of R.

Electric field in a dielectric is inversely proportional to the dielectric permittivity ε. Therefore, the reorganization energy is expected to decrease with increase of ε. The polarization of solvent molecules has a fast electronic component (at visible or ultraviolet light frequency) and a slow ionic reorientation component (at microwave or radio frequency). Correspondingly, the dielectric permittivities at both characteristic frequencies enter the equation for the reorganization energy [84,85,24],

$$\lambda = \Delta e^2 \left(\frac{1}{2a_1} + \frac{1}{2a_2} - \frac{1}{R} \right) \left(\frac{1}{\varepsilon_0} - \frac{1}{\varepsilon_s} \right), \qquad (9)$$

where a_1 and a_2 are the radii of reacting molecules (modeled as spheres), R is the distance between the centers of the molecules, Δe is the transferred charge, ε_0 is the dielectric permittivity at optical frequency, and ε_s is that at low frequency (nearly static).

The reorganization energy enters the formula for the reaction rate constant k as [24,84,85,]

$$k = A\exp\left(-\frac{\lambda\left(1+\Delta G_0/\lambda\right)^2}{4k_BT}\right), \tag{10}$$

where T is the temperature, k_B is the Boltzmann constant, ΔG_0 is the standard free energy of the reaction and A is the pre-exponential factor depending on the nature of the electron transfer. (Note that one of the most counterintuitive predictions of the Marcus theory – slowing down of the electron transfer kinetics in the inverted region, where it becomes thermodynamically highly favorable – was the aim of recent Ref. [86], focused on concerted proton-electron transfer reactions in the latter regime.)

The Marcus theory was originally developed for redox reactions in homogeneous dielectric media (solvents) and later extended to photosynthesis [85], corrosion [87], chemiluminescence [88], and charge separation in organic solar cells [89]. We asked the question [24] whether the reorganization energy and the rates of chemical reactions can also be controlled by *non-local* modifications of inhomogeneous dielectric environments. This motivated the studies discussed in Part II below.

PART II. EXPERIMENTAL DEMONSTRATIONS

Control of emission with hyperbolic metamaterials

Control of spontaneous emission As it has been predicted in Ref. [10], metamaterials with hyperbolic dispersion (also known as hyperbolic metamaterials) can control both the rate and the directionality of spontaneous emission and enable the design of a single photon gun for quantum optics applications. Two most common morphologies of hyperbolic metamaterials are (i) arrays of parallel metallic nanowires grown in pores of anodic alumina membranes and (ii) lamellar stacks of subwavelength alternating metallic and dielectric layers. In line with the theoretical predictions, it has been experimentally demonstrated that these two geometries can enhance the rates of spontaneous emission of quantum dots [6,11,13], dye molecules [7,8,9,14,90] and vavancy centers in diamond [91] deposited onto hyperbolic metamaterials, Fig. 8. The effect appeared to be stronger on top of nanowire-based metamaterials [7] than lamellar metal-dielectric metamaterials [6,8,9,11]. An even higher rate of the spontaneous emission decay can be obtained if emitting centers are embedded in dielectric layers inside the volume of the metamaterial slab [9,13] or deposited on top of its nanopatterned surface [14].

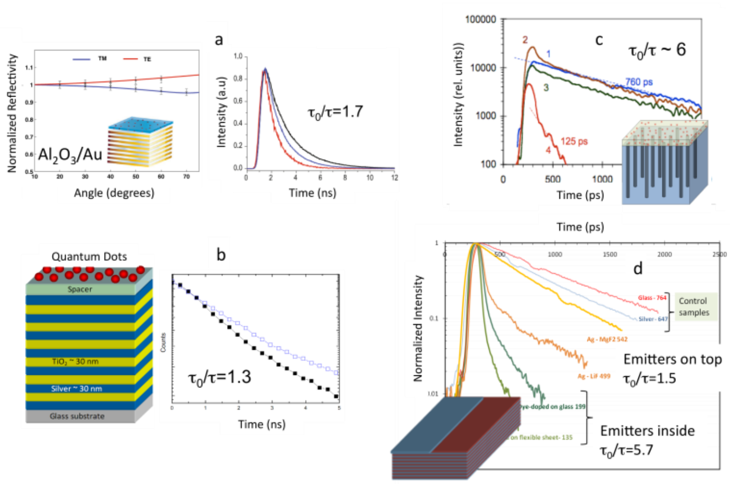

Fig. 8. Shortening of spontaneous emission lifetime τ with hyperbolic metamaterials. The geometry of the metamaterial and the emission decay time shortening, τ_0/τ, are indicated in the figures. (Here τ_0 is the emission lifetime in a control sample.) Adopted and adapted from Ref. [8] (a), Ref. [6] (b), and Ref. [7] (c).

The photonic density of states (or the Purcell enhancement factor) determined by hyperbolic metamaterials is not spectrally flat but rather has a strong dispersion [12,13,48]. This causes modification of the spontaneous emission spectra, exemplified by the blue shift of the emission spectral band experimentally demonstrated in Ref. [15], Fig. 9. (Note that the spectral shift in this particular experiment has nothing to do with alteration of energy eigen-values routinely observed in a strong coupling regime [74,75,76].)

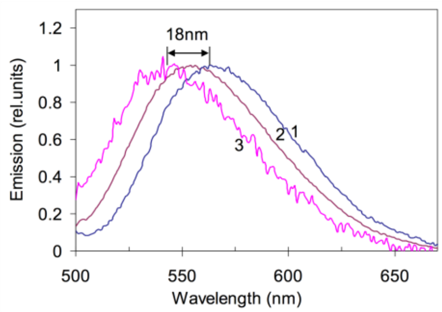

Fig. 9. Blue shift of spontaneous emission with hyperbolic metamaterial. Experimental emission spectrum of DCM doped PMMA deposited on glass (1), embedded in the hyperbolic metamaterial with PMMA as the outmost layers (2), and embedded in the hyperbolic metamaterial with Ag as the outermost layer (3). Adopted from Ref. [15].

Control of stimulated emission In line with [92,93,94,95], optically pumped stimulated emission of surface plasmon polaritons (without intentional feedback) can be achieved in dye-doped polymeric films on top of metallic substrates. In Ref. [96], Kitur et al. studied stimulated emission in HITC(dye):PMMA(polymer) films deposited on top of Ag and lamellar metal-dielectric (Ag/MgF_2) metamaterial with hyperbolic dispersion. The stimulated emission in the samples studied was evidenced by narrowing of the emission spectrum and a threshold in the input-output dependence. Remarkably, (i) the stimulated emission threshold on top of the metamaterial substrate was lower (between 2.5-fold and 7-fold in different samples) than on top of the silver film, and (ii) the laser spectral line on top of the metamaterial was red-shifted in comparison to that on Ag. In tunable lasers, featuring partly overlapping absorption and emission bands, the reduction of the threshold and red shift of the stimulated emission line are characteristic of a higher gain (or a smaller loss) in the system [95]. This behavior of the multimode plasmonic laser, in Ref. [96], is consistent with enhancement of the photonic density of states in a hyperbolic metamaterial.

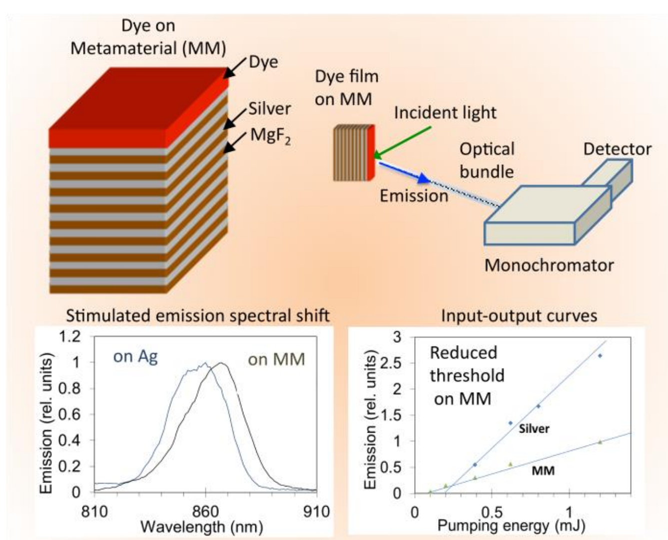

Fig. 10. Top left: Schematics of the sample. Top right: Experimental setup. Bottom left: stimulated emission line on top of Ag and on top of hyperbolic metamaterial. Bottom right: Input-output curves measured on top of Ag and metamaterial demonstrating reduced threshold on top of the metamaterial. Adopted from Ref. [96].

Control of energy transfer with nonlocal metal-dielectric environments

State of the Art In homogenous dielectric media, the rate of spontaneous emission increases ($A \propto n$ [28]) while the rate of the Förster energy transfer (in a pair of donor and acceptor) decreases ($W \propto n^{-4}$, Eqs. 4 and 5 [54]) with increase of the refractive index n. Therefore, the same dielectric environments, which inhibit spontaneous emission, can be expected to boost the energy transfer. This poses two questions: (i) whether the energy transfer can be controlled by PDOS, which also depends on n (Eq. 1 [28]), and (ii) whether it can be further tuned by engineered nanostructured non-local dielectric environments, including plasmonic nanoparticles, metallic mirrors, metamaterials and other nanophotonic systems.

The literature has several contradictory theoretical and experimental studies of the effect of the local PDOS on the Förster energy transfer. Thus, the latter was claimed to be dependent on [97,17,98,99,100] or independent of [101,102,103] the photonic environment. Experimentally, high density of photonic states was reported to enhance the energy transfer rate in cavities [17], modulate it [98,99,] leave it unaffected [101,102,103] in vicinity of mirrors and planar interfaces, or inhibit it in plasmonic nanostructures [104]. This broad range of claims and opinions made the studies outlined below particularly important.

Energy transfer between two molecules separated by a DNA molecule In the study [18], donor and acceptor molecules (Atto488 and Atto565, respectively) were attached to two opposite sides of a DNA, maintaining constant distance between donor and acceptor, Fig. 11a. The emission kinetics of donors in the presence and in the absence of acceptors, which allowed the authors [18] to deduce, correspondingly, the rates of the energy transfer and of the spontaneous emission, were measured at different distances from the metallic mirror in minima and maxima of the periodically changing PDOS (termed as LDOS), Figs. 11b and 11c. It has been concluded that, within the experimental error, the rate of the energy transfer was independent of PDOS. This experimental result was in agreement with the theoretical prediction (based on the Green function calculations) for single donor molecule and single acceptor molecule interacting in vicinity of a mirror [18].

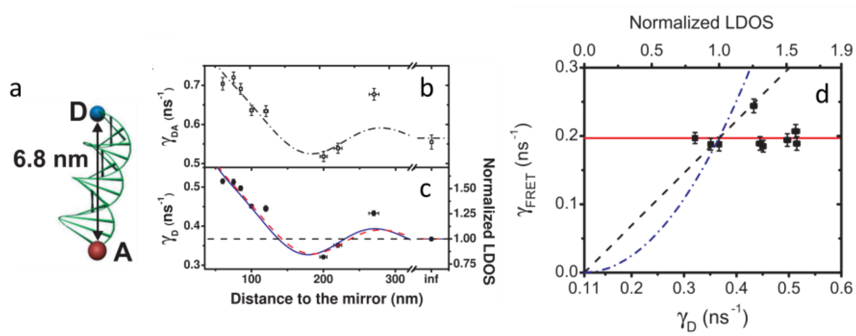

Fig. 11. (a) Donor (Atto488) and acceptor (Atto565) dye molecules separated by 6.8 nm DNA strand. (b) Total donor decay rate γ_{DA} oscillates with distance to the mirror. Dash-dotted curve: model consisting of the calculated PDOS, averaged over the whole donor emission band, plus a constant energy transfer rate γ_{ET}. (c) The total decay rate γ_D of the donor-only samples shows the well-known oscillation as a function of distance d to the mirror. (d) Förster energy transfer rate γ_{ET} is independent of the donor-only decay rate γ_D that is proportional to the normalized PDOS at the donor emission frequency. Adopted from Ref. [18].

Effects of the metallic and metal-dielectric substrates on the energy transfer In Ref. [19], the effect of metallic and lamellar metal-dielectric metamaterial surfaces on the energy transfer was studied in thin, 33 nm to 100 nm, (PMMA) films co-doped with donor (DCM dye, 2×10^{19} cm^{-3}) and acceptor (DOTC dye, 1.2×10^{19} cm^{-3}) molecules. In DCM:DOTC:PMMA films deposited on glass, emission of acceptors, at ~720 nm, was observed at excitation of donors at 400 nm, Fig. 12a. Furthermore, the emission kinetics of donors were shown to be different (much shorter) in the presence of acceptors than in the absence of acceptors, Fig. 12b. This was a proof of the efficient donor-acceptor energy transfer on top of glass.

When the same experiments were repeated in similar DCM:DOTC:PMMA films deposited on top of Au, Ag or lamellar (hyperbolic) metamaterial substrates, (i) no emission of acceptors was observed at the excitation of donors, Fig. 12a, and (ii) the emission kinetics of donors in the presence of acceptors slowed down in comparison to those on glass, Fig. 12b. These observations suggest that the donor-acceptor energy transfer is inhibited in vicinity of metallic and lamellar metamaterials surfaces.

When the rates of spontaneous emission of donors, in the absence of acceptors, were compared against the rates of energy transfer from donors to acceptors, it was found that the same nonlocal dielectric environments, which boost spontaneous emission, also inhibit the energy transfer, Fig. 12c. This conclusion is in agreement with the line of reasoning formulated for homogeneous media in the beginning of this section. However, it does not directly relate the rate of the energy transfer with PDOS. Thus, the theoretical study [19] of the effect of a metallic surface on the rate of the energy transfer between individual donor and acceptor molecules failed to describe the experimental results quantitatively and, in agreement with Ref. [18], has shown no correlation between the energy transfer and PDOS.

As discussed below, it has been inferred that the observed phenomenon can be explained in terms of strong coupling and coherent behavior of large ensembles of donor and acceptor molecules and/or collective coupling of these ensembles with surface plasmon polaritons supported by metal/dielectric interfaces.

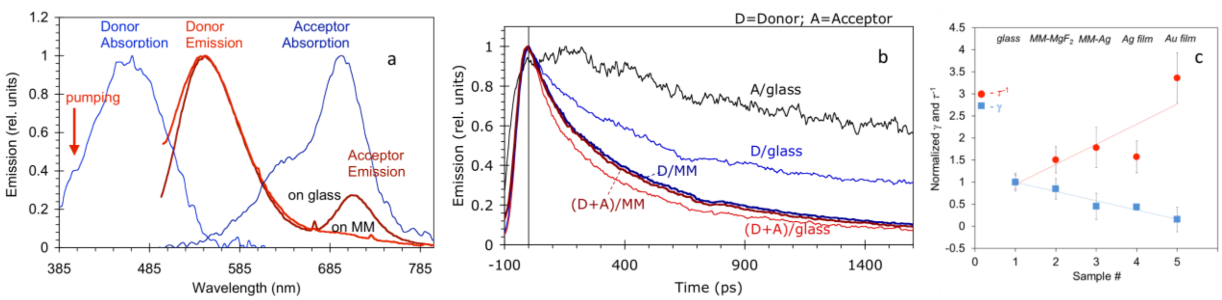

Fig. 12. (a) Emission spectra of ≈80 nm thick PMMA films co-doped by DCM and DOTC molecules, deposited onto glass (1) and hyperbolic metamaterials (2) substrates and pumped at λ=400 nm into the absorption band of DCM. (b) Spontaneous emission kinetics in PMMA films deposited on glass: donors (DCM) in a singly doped PMMA film (1, D/glass), donors in the PMMA film co-doped with donors and acceptors (2, D+A/glass), and acceptors (DOTC) in the PMMA film co-doped with donors and acceptors (3, A/glass). Spontaneous emission kinetics in PMMA films deposited on metamaterial substrates with Ag as the top layer: donors (DCM) in a singly doped PMMA film (4, D/MM) and donors in the PMMA film co-doped with donors and acceptors (5, D+A/MM). All films were pumped into the absorption band of acceptors at λ=392 nm. (c) Emission decay rates and Förster energy transfer constants γ in dye-doped films deposited on top of glass (1), metamaterial with MgF_2 as the outermost layer (2), metamaterial with Ag as the outermost layer (3), Ag film (4), and Au film (5). Adopted from Ref. [19].

Control of concentration quenching with nonlocal dielectric environments The effect of lamellar hyperbolic metamaterials and metal/dielectric interfaces on the concentration-dependent luminescence quenching in thin polymeric poly (methyl methacrylate) (PMMA) films doped with HITC dye molecules (2-7-(1,3-dihydro-1,3,3-trimethyl-2H-indol-2-ylidene)-1,3,5-heptatrienyl-1,3,3-trimethyl-3H-indoliumiodide) has been studied in Refs. [105,106]. Experimentally, thin (~80 nm) HITC:PMMA films were deposited onto glass, silver and lamellar metal/dielectric metamaterials (which had hyperbolic dispersion at λ>384 nm [19]) and optically pumped at λ=795 nm with ~150 ns pulses of a mode-locked Ti:sapphire laser. The emission kinetics, recorded at λ>850 nm with a Vis-IR streak camera, were found to shorten with increase of the dye concentration, Fig. 13a. The rate of this concentration quenching (energy transfer to quenching centers) was approximately proportional to the square of the dye concentration, Fig. 13b. This finding is consistent with the assumption that (i) the quenching centers are pairs of aggregated dye molecules or (ii) the energy transfer to acceptors is assisted by the migration of excitation over donors [54].

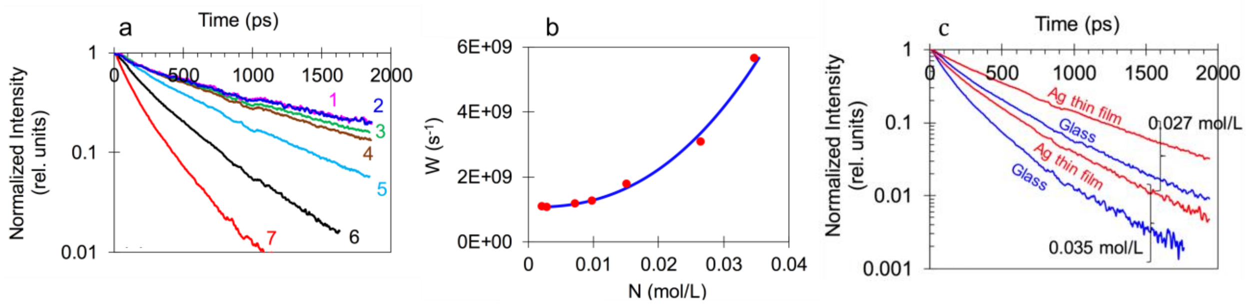

Fig. 13. (a) Emission kinetics of HITC:PMMA films deposited on glass at short-pulsed laser pumping at different dye concentrations: 0.002 mol/L trace 1, 0.003 mol/L trace 2, 0.007 mol/L trace 3, 0.010 mol/L trace 4, 0.015 mol/L trace 5, 0.027 mol/L trace 6, and 0.035 mol/L trace 7. (b) Concentration dependence of the emission decay rates (on top of glass); red circles – experiment, solid line – fitting with the formula $W=A+BN^x$. (c) Emission kinetics of HITC:PMMA films on silver and glass substrates at the dye concentrations equal to 0.035 mol/L and 0.027 mol/L. Adopted from Ref. [105].

In line with Ref. [19], the concentration quenching (energy transfer) was found to be inhibited in vicinity of metallic films and lamellar metal-dielectric metamaterials. (The effect of metamaterials was marginally larger than that of the silver substrates.) The inhibition of the concentration quenching decreased with increase of the size of the spacer, MgF_2, separating the dye-doped film and the metallic surface. The characteristic length-scale of the inhibition (the distance between the dye molecules and the metallic surface, at which the inhibition becomes significant) was found to be ~47 nm. It was much longer than the Förster radius (the characteristic distance of the donor-acceptor energy transfer, 5 nm to 7 nm), and smaller than the penetration of the surface plasmon polariton field to the dielectric (≥250 nm).

In both Refs. [19] and [105], the characteristic system dimensions, *e.g.* the thicknesses of the dye-doped films and the average distance between dye molecules and the metallic surfaces, were much larger than the Förster radius. Therefore, the observed inhibition of the energy transfer cannot be explained in terms of the model [18],[19] taking into account individual donor and acceptor centers affected by the presence of the metal. At the same time, the character of the donor-acceptor energy transfer is predicted to change dramatically if the electromagnetic coupling between donor molecules, leading to formation of a coherent collective state, is taken into account [12].

At high concentration of HITC molecules used in the experiment (0.053 mol/L in solid state) [105,106], the coupling between the ensemble of dye molecules and SPPs was strong enough to produce 0.14 eV Rabi splitting of the SPP dispersion curve observed in the Kretschmann reflectance experiment, Figs. 14a,b.

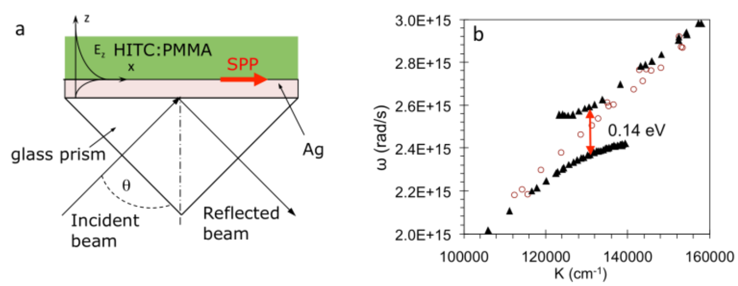

Fig. 14. (a) Kretschmann geometry setup for study of the SPP dispersion and the strong coupling. (b) SPP dispersion curves measured when the PMMA film is not doped (empty circles) and doped with HITS dye in concentration 0.053 mol/L (filled triangles). The latter curve demonstrates the Rabi splitting of 0.14 eV, which characteristic of strong exciton-plasmon coupling. (The thickness of the polymer film is ~ 1 µm and the thickness of the Ag film is 32 nm). Adopted from Ref. [106].

Strong coupling of dye molecules with plasmonics substrates is known to cause coherent spontaneous emission [75,79], manifesting formation of a collective state of donors – the phenomenon enabling long-range control of the energy transfer with an external mirror [12]. On the other hand, the strong coupling affects energy eigenvalues of the hybridized states and, therefore, can change spectral overlap of the emission band of donors and the absorption band of acceptors, leading to a change in the energy transfer rate, Eq. 5. Therefore, the adequate description of the systems studied is likely to be sought in terms of the model taking into account coupling of donor and acceptor ensembles to surface plasmons and, through coupling with plasmons, to each other.

(Note that the spectral overlap of the emission of donors and absorption of acceptors can also be caused by interaction of molecules with their mirror images [107]. This possible explanation of the experimentally observed inhibition of the energy transfer in vicinity of metallic surfaces requires thorough theoretical investigation.)

Long-range wetting transparency on top of layered metal-dielectric substrates

The authors of Ref. [21] have experimentally studied wetting of several metallic, dielectric and lamellar metal/dielectric substrates, including glass, thin and thick Au films, and Au/MgF_2 stacks (both pristine and coated with MgF_2 layers of varied thickness). In general, van der Waals forces are not the only contributors to the surface energy and the wetting angle. Other important inputs come from *e.g.* material-specific surface energy, determined by polarization and chemical activity of the top molecular layer of the substrate [69,108]. Therefore, a series of wetting experiments has been designed, in which the topmost layer of the solid-state substrate that was in direct contact with the water droplet was kept the same, and the underlying medium as well as the corresponding distribution of non-local dielectric permittivity was changed in a systematic manner (Fig. 5) by *e.g*. changing the thickness of the topmost MgF_2 film.
It has been found that the wetting angle on top of thick, l≥100 nm to l≥400 nm, MgF_2 layers is ≤10°, approximating the total wetting condition. At the same time, wetting angles on top of pristine glass, Au films and Au/MgF_2 metamaterials (with Au outmost layer) are significantly larger, ≥65°. Remarkably, as layers of MgF_2 of varied thickness are deposited on top of glass, Au or Au/MgF_2 metamaterial, the contact angle does not change abruptly from the one corresponding to the underlying substrate to the one corresponding to thick MgF_2. It has been, thus, concluded (to some surprise) that the wetting angle is nearly insensitive to the chemical nature of the immediate substrate and its surface. Instead, as the thickness of the MgF_2 layer is gradually increased from l=0 nm (no MgF_2) to l>100 nm, the wetting angle changes smoothly and continuously, demonstrating sensitivity to the presence of underlying substrate at the thickness of the MgF_2 layer of the order of ~100 nm, Fig. 15. This phenomenon is referred to as long-range wetting transparency.

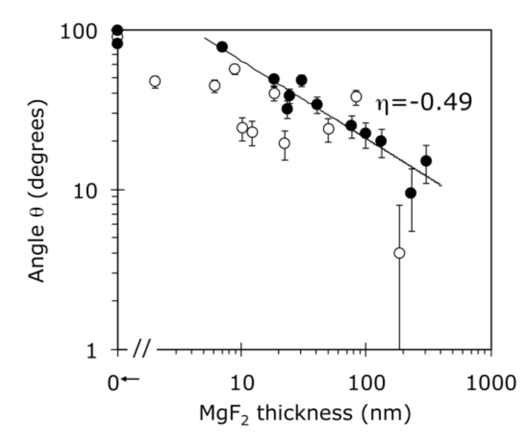

Fig. 15. Wetting angles measured on top of MgF_2 films of different thickness deposited on thin (closed circles, average thickness 51 nm) and thick (open circles, average thickness 103 nm) Au films. Vertical error bars (±4 degrees) are shown. Horizontal error bars are smaller than the size of the characters. Adopted from Ref. [21].

The semi-qualitative analysis suggests that if the interaction energy of two parallel slabs changes with the distance as l^{-2} (the behavior predicted by the most simple model of dispersion van der Waals interactions), the wetting transparency, although possible, should not extend longer than several nanometers [21]. The gradual change of the wetting angle occurring over tens of nanometers of the MgF_2 spacer [21] can be partly due to the thickness dependence of the MgF_2 refractive index. However, it is unlikely that this effect can fully account for the whole magnitude of observed phenomenon (change of θ from $\geq 65^o$ to $\leq 10^o$). It has been inferred [21] that the experimentally observed long-range wetting transparency can possibly be due to strong distance dependence of the Hamaker function, which determines the strength of the dispersion van der Waals-London interactions related to retardation of electromagnetic radiation.

Control of chemical reactions in a weak coupling regime

Control of photodegradation of semiconducting polymer P3HT with metallic and lamellar metal-dielectric substrates As it has been discussed in the introduction and several subsequent sections, proximity to metallic surfaces, plasmonic structures, cavities and other inhomogeneous dielectric environments is known to control spontaneous emission, energy transfer, wetting, and many other phenomena of practical importance. The aim of the study [24] was to demonstrate that, in spirit of the Marcus theory, the rates of chemical reactions can, too, be influenced by nonlocal dielectric environments, such as metallic films and metal/dielectric multilayer structures. The chemical reaction studied in Ref. [24] was photodegradation of the semiconducting polymer P3HT, which is the material of choice in many organic photovoltaic devices [109]. Under photoexposure in an ambient atmosphere, the P3HT absorption band at ~550 nm is getting smaller (due to photodegradation of thiophene rings forming the polymer) and shifts to the blue range of the spectrum (due to shortening of polymeric chains) [110],[111], Fig. 16.

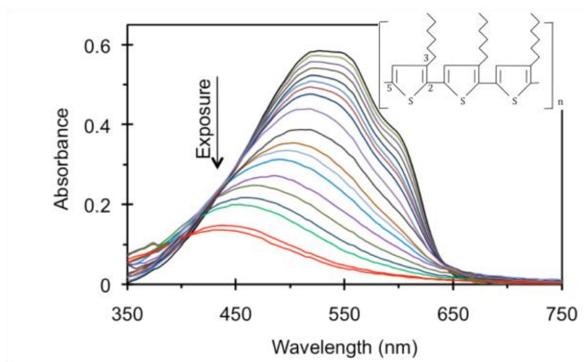

Fig. 16. Absorbance spectra (natural logarithm) of the 23 nm thick regioregular P3HT film deposited onto a glass substrate with thick Ag film on the back (measured in the reflection experiment). The shoulder at ~610 nm and two (not well resolved) peaks at ~525 nm and ~555 nm are the signature of a quasi-ordered structure. Inset: Regioregular 2,5-poly-3-hexyl-thiophene (P3HT) polymer. Adopted from Ref. [24].

In the photo-oxidation studies, P3HT films were deposited on a variety of substrates, including glass, Ag, Au and Al films, Ag/MgF_2 lamellar metamaterial (with Ag as the topmost layer) and all the same substrates coated with 25 nm MgF_2 layers. In the photodegradation experiments, the samples were exposed to a white light illumination by a 50 W halogen lamp. The total exposure time approximated 100 hours. During this period, the absorbance spectra of the p3th films were measured multiple times in the transmission and reflection experiments. After proper normalization, the latter spectra were equivalent to transmission spectra of the P3HT films of double thickness.

With increase of the light exposure, the P3HT absorption band was getting smaller (due to reduced number of survived thiophene rings) and its maximum position experienced a blue shift (due to shortening of the π conjugated P3HT polymer chains). When the absorbance and the wavelength corresponding to the maximum of the absorption band were plotted against the exposure time, they resulted, respectively, in the absorption decay kinetics (Fig. 17) or the spectral shift kinetics (inset of Fig. 17).

It has been found [24] that (i) the rates of photodegradation (reduction of absorption and the frequency shift) are smaller on top of metallic films and lamellar metal/dielectric substrates, covered with a thin insulating MgF_2 layer, than on top of purely dielectric substrates, glass and MgF_2, Fig. 18. (The latter rates were corrected for interference effects, spectral sensitivity of photodegradation, and emissivity of the lamp used to photo-expose the samples.) This central observation of Ref. [24] proves that chemical reactions, *e.g.* photodegradation of P3HT, can be controlled by nonlocal dielectric environments. (ii) At the same time, the rates of photodegradation of P3HT films deposited directly onto metallic substrates were higher than those in purely dielectric reference samples. The latter effect can be partly due to a conventional catalysis [112,113,114], Fig. 18. (iii) The type of metal (*e.g.* Ag, Au or Al) used to fabricate metallic and metal/dielectric substrates affects the ratio between the rate of reduction of absorption and the rate of the blue shift. Interestingly, the order of the latter ratios correlated with the order of dielectric permittivities in the metals studied [24], inset of Fig.18. (In a separate study [115], it has been shown that the rate of photodegradation of P3HT does not correlate with the substrate-specific excited state concentration and spontaneous emission of thiophene rings.)

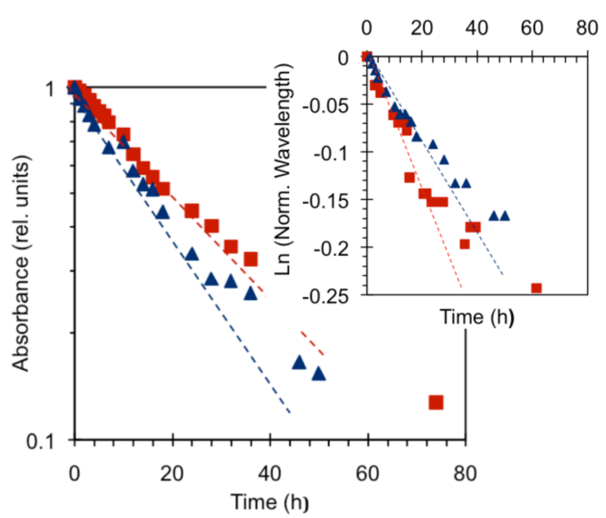

Fig. 17. Dependence of the maximal absorbance on the exposure time in the P3HT films deposited on glass (squares) and Ag/MgF_2 metamaterial with Ag on top (triangles). Inset: Dependence of the (normalized to one) wavelength of the absorption maximum on the exposure time, measured in the same samples as in the main frame. Adopted from Ref. [24].

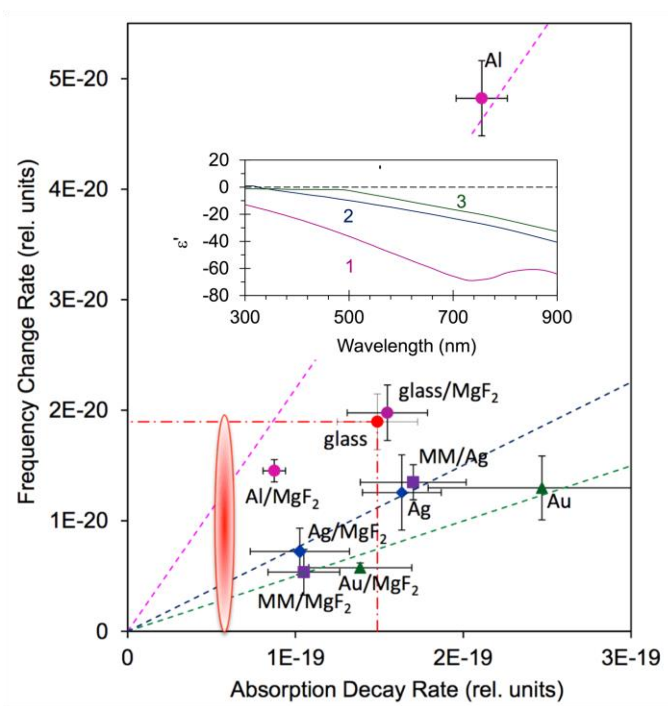

Fig. 18. The rate of the reduction of absorbance plotted against the rate of the frequency shift of the absorption maximum. The rates are normalized to the corresponding effective pumping intensities. Inset: Spectra of real parts of dielectric permittivities in Al [116] (trace 1), Ag [117] (trace 2), and Au [117] (trace 3). Red ellipse shows the reduction of the absorption decay rate in the strong coupling regime (as it is discussed in the section Control of Chemical Reactions in a Strong Coupling Regime below). Adopted and adapted from Ref. [24].

Thus, it has been unambiguously proven [24] that the rates of chemical reactions can be controlled not only by *local* dielectric permittivities, but also by *non-local* dielectric environments. This important step toward understanding of a complex relationship between chemical reactions and nonlocal dielectric environments has been followed by the theory development and a broader scope of thorough experimental studies [26], as discussed below.

Effect of lamellar metal-dielectric substrates on a charge transfer The effect of lamellar metal-dielectric hyperbolic metamaterial substrates on the charge transfer in a thin layer of triphenylene:perylene diimide dyad supramolecular self-assemblies (Figs. 19 a,c) has been demonstrated in Ref. [26]. Thus, in the vicinity of the metamaterial surface (Fig. 19b), the rate of charge separation decreased by a factor of 2.4, while the rate of the charge recombination got reduced by a factor of 1.7. (The inhibition has been shown to increase with increase of the number of pairs of metal and dielectric layers.) This experimental result was explained in terms of the modified Marcus theory taking into account mirror images of the interacting molecular dipoles. It has been argued that the latter non-local effect influences the energy of dipole-dipole interaction, the reorganization energy λ [26] and the rate of the charge transfer the same way as the modified local dielectric permittivity □ (*e.g.* dielectric permittivity of a solvent) would do. A good agreement of the model and the experiment as well as a qualitatively similar result obtained in the PH3T:PC60BM system [26] show the generality of this non-local phenomenon and suggest that a wide range of kinetic tailoring opportunities can arise from substrate engineering. This work paves the way toward the design of artificial substrates to control CT dynamics of interest for applications in optoelectronics and chemistry.

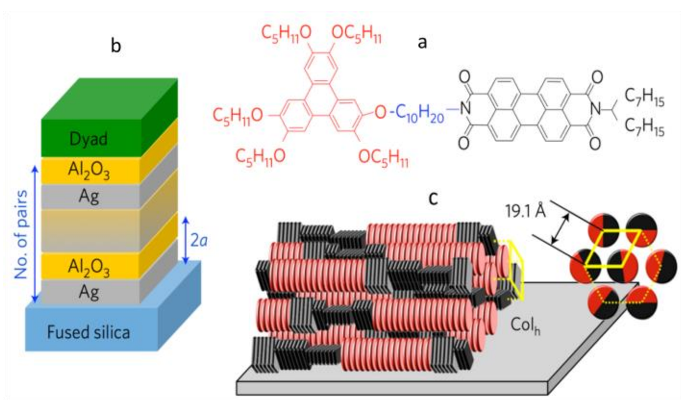

Fig. 19. (a) Schematics of the Ag/Al_2O_3 hyperbolic metamaterials structure with donor and acceptor molecules (diads) on top. (b) Triphenylene:perylene diimide dyad (TriPh: PerDi) composed of discotic mesogenic conjugated units. (c) Connected by a decyloxy flexible bridge, the TriPh (D) and PerDi (A) units are prone to self-assemble in a solid-state multi-segregated D–A columnar structure. Spontaneous planar orientation of columnar hexagonal structures (Colh) consisting of domains of lying columns. Adopted from Ref. [26].

Control of chemiluminescence In pursuit of alternative classes of chemical reactions that can be controlled with nonlocal metal/dielectric environments, Peters et al. [118] studied chemiluminescence kinetics a series of thin R6G:DNPO:PMMA films deposited onto a variety of metallic, metal/dielectric and dielectric substrates. Here peroxyoxalate Bis(2,4-dinitrophenyl) oxalate (DNPO) is one of the most efficient nonenzymatic chemiluminescent reactants [119], for which chemiexcitation proceeds via the chemically initiated electron-exchange luminescence mechanism [119,120] (Fig. 20), rhodamine 6G (R6G) dye is an emitter, and poly(methyl methacrylate) (PMMA) is a host polymer. The experimental samples, R6G:DNPO:PMMA films deposited onto metal/dielectric substrates, were mounted on the end of the rod attached to the inner side of a lid closing a glass jar, Fig. 21a. The jar was partly filled with an H_2O_2 solution and the R6G:DNPO:PMMA films were exposed to the H_2O_2 vapor. The chemiluminescence emission kinetics were collected and analyzed as explained below.

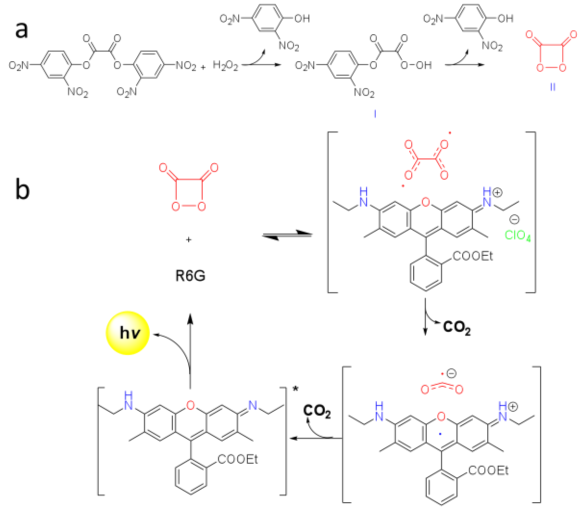

Fig. 20. (a) Rapid reaction between hydrogen peroxide and DNPO produces monoperoxide 2-(2,4-dinitrophenoxy)-2-oxoethaneperoxoic acid (I), which undergoes an intramolecular nucleophilic displacement reaction to give 1,2-dioxetanedione (II). (b) Thermolysis of 1,2-dioxetanedione generates the S = 1 oxalate biradical, which oxidizes R6G to R6G•+ and decomposes to give CO_2 and S = 1/2 CO_2•- . Back electron transfer (BET) ensues to yield CO_2 and excited R6G*, which emits upon relaxation. Adopted from Ref. [118]

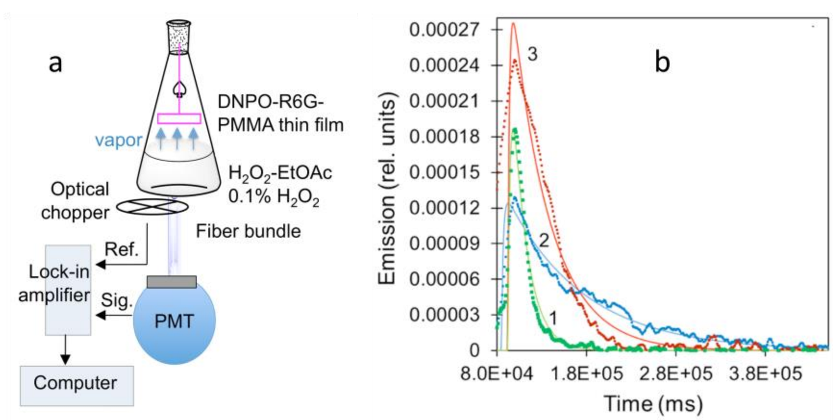

Fig. 21. (a) Schematics of the experimental setup for the chemiluminescent reaction and emission measurement. (b) Emission kinetics of chemiluminescence (in vapor) on top of Ag (trace 1), Ag covered with a thin film of MgF_2 (trace 2), and MgF_2 (trace 3). Adopted from Ref. [118]

We found that when the R6G:DNPO:PMMA films were exposed to H_2O_2 vapor, chemiluminescence kinetics on top of Ag and Au films covered by insulating MgF_2 layer were shorter than those on top of purely dielectric substrates, MgF_2 films on glass, Fig. 21b. In line with the modified Marcus theory [26], it has been inferred that Ag- and Au- based substrates with insulating MgF_2 layer deposited on top affected the reaction rates by influencing polarization energies of reactants and surrounding molecular dipoles. At the same time, the chemiluminescence kinetics on top of Ag and Au surfaces (without insulating MgF_2 spacer) were substantially shorter than those on top of dielectric substrates, probably because of conventional chemical catalysis [112,113,114].

A qualitatively similar behavior was observed on top of Au-based thin films and lamellar metamterial substrates. However, chemiluminescence decay times on top of the metamaterials were slightly shorter than those on top of single Au films and Au/MgF_2 substrates.

The peak emission intensities on top of metallic substrates (with and without MgF_2 layer on top) were lower that those on top of purely dielectric substrates, most likely, due to inhibition of the energy transfer to acceptors (R6G dye molecules) known in vicinity of metals. The further reduction of the chemiluminescence intensity on top of lamellar metal/dielectric stacks could be due to preferential emission of light inside the volume of the metamaterial rather than outside.

To summarize this section, three very different chemical reactions were demonstrated to slow down in vicinity of metallic and metal-dielectric substrates covered by a thin insulating MgF_2 layer. This phenomenon can be tentatively explained by change of dipole interaction and reorganization energies in presence of metallic reflecting surfaces.

Control of chemical reactions in a strong coupling regime

State of the Art Strong and, in particular, ultra-strong coupling have been reported to modify the surface potential [121], electrical conductivity [122], exciton transport [123],[124], Raman scattering [125,126,127] and energy transfer beyond the Förster regime [128]. Of particular interest to the study [25] discussed below was the effect of strong coupling on chemical reactions. Thus, control of a photoisomerization reaction with the strong coupling to a Fabry-Perot cavity and reversible all-optical switching between two isomers, spiropyrane and merocyanine, have been demonstrated in the pioneering studies [22,23]. A more recent example of the effect of strong coupling of J-aggregated TDBC [129] organic dye molecules with triangular silver nanoprisms, resulting in hundredfold reduction of the photodegradation rate, has been reported in Ref. [130]. The effect of strong coupling on photochemical reactions (the type of reaction researched in the study [25]) was explained in the literature in terms of altered landscapes of electronic excited and ground states [23],[131], modification and creation of avoided crossing energy gaps [131],[132], and increase of relaxation rates of hybridized states [130]. Strong coupling of a coherent molecular ensemble to a cavity mode was also shown to trigger many-molecule reactions with a single photon [133].

Furthermore [25], strong coupling of a cavity with an electronic transition was predicted to decouple collective electronic and nuclear degrees of freedom in a molecular ensemble, leading to enhancement or suppression of intramolecular electron transfer by orders of magnitude in comparison with free space [134]. As photochemical reactivity critically depends on strong coupling involving *excited* molecular electronic states, a much larger class of ground state reactions are controlled by strong coupling of vibrational states to the vacuum electromagnetic field in a cavity [135,136,137]. Thus, the ground-state deprotection of a simple alkynyl-silane, has shown fivefold reduction of the reaction rate when the Si-C vibrational stretching modes of the reactant were strongly coupled to the resonant IR cavity [137]. The progress and trends in the polariton chemistry are reviewed in recent Ref. [138].

Photodegradation of the semiconducting polymer P3HT in the strong coupling regime As it has been shown above, redox chemical reactions, such as photodegradation of the semiconducting polymer P3HT, can be controlled by a (*weak*) coupling with nonlocal metal/dielectric environments. On the other hand, *strong* coupling of quantum wells, quantum dots and dye molecules with resonant cavities and surface plasmons enables and affects scores of physical phenomena, including chemical reactions (see references in the section above). In Ref. [25], Peters et al. have combined the two phenomena and demonstrated that under tungsten lamp illumination, strong coupling of the semiconducting polymer P3HT with a resonant cavity (characterized by the gigantic Rabi splitting of 1.0 eV) causes threefold reduction of the rate of photodegradation.

The experimental setup and the measurements in the study [25] were similar to those in Ref. [24]. The absorption spectra of P3HT films on glass (Fig. 22a) and the reflectance spectra of resonant Fabry-Perot cavities filled with P3HT polymer (Fig. 22b) were measured after numerous light exposures (with Tungsten lamp), over several tens of hours. The observed reduction of the absorption band and the change in the spectral positions of the dips in the reflection spectra (corresponding to two polariton branches in the strong coupling regime) were used to determine the concentration of remaining thiophene rings as the function of time and light exposure. The resultant kinetics (Fig. 23) were used to calculate the rates of photodegradation of P3HT in Fabry-Perot cavity as well as control samples.

The latter rates were further normalized by (i) the action spectrum of the P3HT photodegradation, (ii) the emissivity spectrum of the lamp, (iii) the spectrum of the light intensity integrated over the P3HT film's thickness, (iv) reduction in the oxygen flow caused by the top silver mirror, and (v) possible effect of chemical catalysis. The reported three-fold effect of the resonant cavity (in the strong coupling regime), which was presumably dominated by the singlet oxygen mechanism [111], was larger than that of the Ag/MgF_2 thin film and lamellar metamaterial substrates [24] (see Fig. 18), manifesting that control of light-matter interaction in the strong coupling regime is more efficient than that in the weak coupling regime.

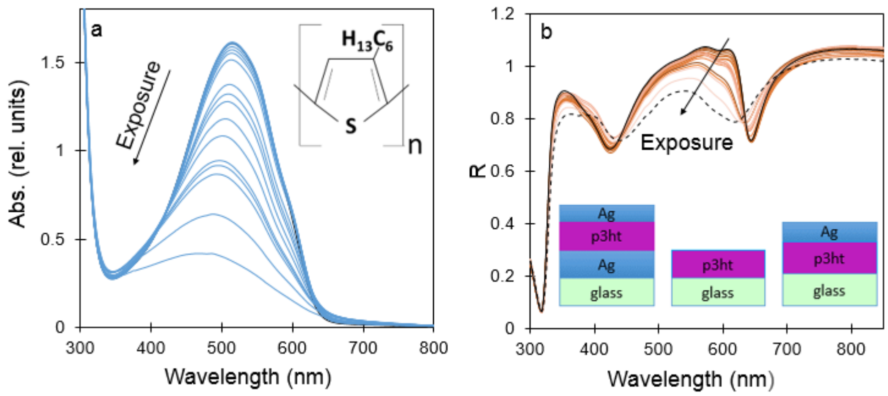

Fig. 22. (a) Transformation of the absorption spectrum of P3HT deposited on glass under tungsten lamp illumination in the presence of oxygen. (b) Same for the reflectance spectrum of the P3HT filled cavity. Inset of Figure 1a: chemical formula of P3HT. Inset of Figure 1b: Schematic of the experimental samples: P3HT in the cavity, P3HT on glass, P3HT on glass covered by a thin semitransparent Ag film. Adopted from Ref. [25].

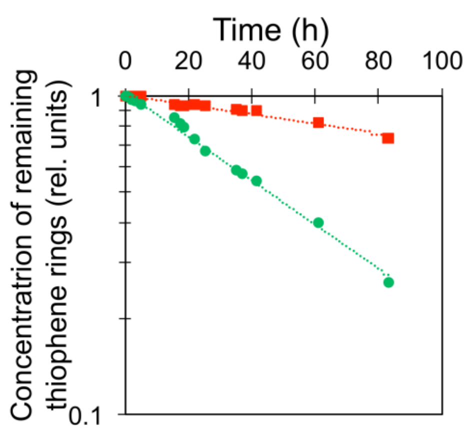

Fig. 23. Photodegradation kinetics of P3HT on glass (circles) and in cavity (squares) under illumination with Tungsten lamp. Adopted from Ref. [25].

Strong coupling with a Farry-Perot cavity causes hybridization of the molecular excited states and the cavity mode [22,23,130,131,132], resulting in formation of the upper (+) and lower (-) polariton branches separated by the Rabi energy $\hbar\Omega$, see the reaction pathways involving single oxygen mechanism [111] without (Fig. 24a) and with (Fig. 24b) strong coupling with the cavity. According to Refs. [130],[139], one of the possible factors contributing to deactivation of $^3P^*$ in organic molecules is the reverse intersystem crossing $^3P^* \rightarrow {}^1P^*$, see Fig. 24b. This process, whose rate is proportional to $\exp(-\Delta E_{ST}/kT)$, is negligibly

small at large energy gap ΔE_{ST} between the singlet and triplet states and its efficiency grows as ΔE_{ST} becomes smaller (here ΔE_{ST} is the energy difference between the singlet and tripled excited states, k is the Boltzmann constant and T is temperature). As it has been claimed in Ref. [139], strong coupling with the cavity lowers the low polariton branch (-), which is of singlet origin, and does not affect the energy position of the triplet state $^3P^*$. Therefore, this process reduces ΔE_{ST} and increases the reverse intersystem crossing, ~$\exp(-\Delta E_{ST}/kT)$, which depopulates the tripled state $^3P^*$.
One can infer that a similar mechanism of depopulation of the excited triplet state $^3P^*$ and slowing down photodegradation of P3HT in the cavity took place in the experiment of Ref [25]. In fact, the cavity in Ref. [25] was resonant with the absorption band of P3HT at ~550 nm, which caused the splitting of the dispersion curve, and "pushed" the low polariton branch down, reducing the energy gap ΔE_{ST}. This hand-waving reasoning is in qualitative agreement with the experimental result [25]. At the same time, this is not the only possible model, and a different mechanism of depopulation of the triplet excited state was claimed to be responsible for the hundredfold suppression of photo-oxidation in Ref. [130]. The quantitative examination of possible photodegradation mechanisms, is the subject of future studies.
One should note that in the vast majority of the literature reports as well as in the experiments discussed above (carried out in both weak and strong coupling regimes) the effect of non-local dielectric environments on chemical reactions is inhibition. This dominating tendency is also calling for its understanding and explanation.

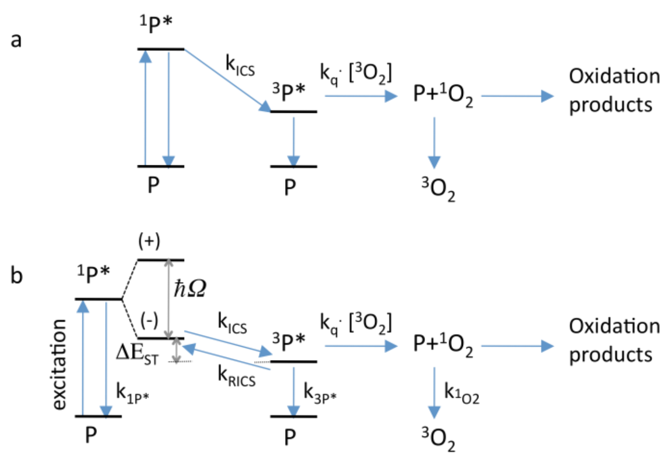

Fig. 24. Scheme of polymer photodegradation by single oxygen. (a) P – ground state of the polymer; $^1P^*$ - excited singlet polymer state; $^3P^*$ – excited triplet polymer state; $^3O_2$ – ground state oxygen; $^1O_2$ – singlet oxygen; k_{1P^*}, k_{3P^*} and k_{1O2} – deactivation constants; k_q – quenching constant; k_r – reaction constant; k_{ISC} – intersystem crossing constant. Horizontal thick black lines represent the energy levels. (b) Same as Figure a, but with the excited state $^1P^*$ split into two polariton branches, (+) and (-), due to interaction with the cavity. $\hbar\Omega$ – Rabi splitting; k_{RISC} – reverse intersystem crossing constant; ΔE_{ST} – energy difference between excited triplet state of the polymer $^3P^*$ and the lower polariton branch (-) of the excited single state of the polymer $^1P^*$. Adopted from Ref. [25].

PART III. Summary

Rationally designed metal-dielectric environments found in photonic (meta) materials and structures can control a broad range of physical and chemical phenomena, which extend far beyond absorption, transmission and reflection of light. A brief review of these exciting phenomena, exemplified by selected experimental studies, was the goal of this Perspective. It was never designed to be comprehensive or all-inclusive, and many related topics, such as plasmonic chemistry [140,141,142,143] hot-electron-induced phenomena [144,145,143], Bose-Einstein condensation of polaritons [146,147,148,149], etc., have not been covered. Interested readers are referred to original research papers and comprehensive reviews, some of which are referenced above.

To summarize, light-matter interactions (of e.g. excitons and resonant cavities or surface plasmons) can occur in both weak and strong coupling regimes [75,76]. The former process affects the rates of electronic transitions, leaving energy eigenvalues of interacting constituents unaltered. On the other hand, strong light-matter interactions affect both the transition rates and the energy eigenvalues.

The phenomenon, which resides at the borderline between optics and quantum physics is spontaneous emission. Its rate can be controlled by the photonic density of states (PDOS, related to the Purcell enhancement factor [29]) in cavities, plasmonic environments, metamaterials and many other metal-dielectric structures, which can be as simple as metal-dielectric interfaces.

In recent years, of particular interest to the research community were metamaterials with hyperbolic dispersion [41,42,43,44], which have a broadband singularity of PDOS and can control the rates [6,7,8,10,11] the spectra [15] and the directionality [10,16] of spontaneous emission. It has also been shown that hyperbolic metamaterials can control not only spontaneous but also stimulated emission [96] (in a dye-doped polymeric film deposited onto lamellar metal-dielectric metamaterial) and reduce the lasing threshold by a factor of two or more.

The rate and the quantum yield of spontaneous emission depend not only on the Purcell enhancement factor but also on the donor-acceptor energy transfer [54], commonly referred as Förster energy transfer [55]. The dependence of the latter on PDOS is the subject of unsettled debates. The three studies of the Förster energy transfer discussed in the section Control of Energy Transfer with Nonlocal Metal-Dielectric Environments indicate that (i) Although the energy transfer rate is theoretically predicted to be independent of PDOS [18,19], the experiments demonstrate that the same metal-dielectric environments, which boost the spontaneous emission, inhibit the energy transfer [19]. (ii) Vicinity of metallic films and lamellar metal-dielectric metamaterials inhibit energy transfer [19,105]. (iii) The characteristic length scale of this effect, ~50 nm [105], is larger than the Förster radius, ~5 to 7 nm, and smaller then the penetration of SPP film to a dielectric, ~ 250 nm. (iv) Due to strong exciton - plasmon coupling taking place at characteristic (high) concentration of dye molecules in the energy transfer experiments, the phenomenon, likely, should be described in terms of collective interaction of an ensemble of donors with an ensemble of acceptors, mediated by SPPs [105].

In wetting experiments, metallic films and lamellar metal-dielectric substrates, separated from a water droplet by a layer of MgF_2, were shown to affect the contact angle when the distance between the water droplet and the metal exceeded tens or even hundreds of nanometers [21]. This long-range wetting transparency can tentatively be ascribed to the effect of non-local dielectric environments on van der Waals interactions. However, this experimental finding is still waiting for its theoretical explanation.

Metal-dielectric substrates (covered with a thin MgF_2 layer) cause inhibition of chemical reactions [24,118], qualitatively similar to an inhibition of the energy transfer. This qualitatively similar behavior was shared by strongly different from each other redox [26], chemiluminescence [118] and photodegradation [24] reactions. The latter inhibition of photodegradation was even stronger in the regime of strong coupling [25] (of semiconducting polymer P3HT with a Fabri-Perot cavity) than in the case of weak coupling with metal-dielectric substrates.

In the regime of weak coupling, the inhibition of redox reactions in vicinity of lamellar metal-dielectric metamaterial substrates can be understood in terms of mirror images of interacting dipoles, modifying the energy of dipole-dipole interactions [26]. At the same time, the inhibition of the photooxidation of P3HT in the strong coupling regime was tentatively explained by the Rabi splitting of the polymer's singlet excite state and enhanced reversed intersystem crossing, which, in turn, caused the reduction of the polymer's triplet excited state participating in the photodegradation reaction [25].

Unique properties of metal-dielectric structures described above and their coupling with ensembles of excitons enable and enhance scores of applications and devices exemplified below. (i) Thus, enhancement of the rate and the quantum yield of spontaneous emission by hyperbolic metamaterials paves the road to development of a single photon gun for quantum optics communication [10]. (ii) Control of energy transfer in weak or strong coupling regimes (assuming that enhancement of an energy transfer is possible) can be used for energy harvesting in a broad range of photovoltaic devices and optical sensors. (iii) Harnessing van der Waals interactions and wetting can lead to design of the new generation of hydrophobic surfaces, with applications ranging from self-cleaning windshields to de-icing of airplanes. (iv) Control of chemical reactions can be essential in a variety of chemical engineering processes as well as materials' stability and resistance to degradation (e. g. corrosion). (v) Finally, many strong coupling phenomena can be employed in the design of optical filters, laser pulse shapers and dispersion-control optics.

To conclude, the studies of light-matter interactions occurring in weak and strong coupling regimes, which affect a broad range of physical and chemical phenomena discussed above, just scratched the surface of a large and intriguing field of research, and scores of exciting discoveries and applications are expected in years to come.

Acknowledgements The authors cordially thank T. V. Shahbazyan, E. E. Narimanov, and A. N. Poddubny for stimulating discussions.

Funding NSF grants 1646789, 1830886, 1856515, AFOSR grant FA9550-18-1-0417, and DoD grant W911NF1810472.

References and Notes

([1]) Raether, H. *Surface Plasmons on Smooth and Rough Surfaces and on Gratings*; Springer-Verlag: Berlin, Heidelberg, 1988.
([2]) Maier, S. A. *Plasmonics: Fundamentals and Applications*; Springer: New York, 2007.
([3]) Engheta, N. and Ziolkowski, R. W. *Metamaterials: Physics and Engineering Explorations*; Wiley, 2006.
([4]) Noginov, M. A.; Podolskiy, V. A., Eds. *Tutorials in Metamaterials* (Series in Nano-optics and Nanophotonics) CRC Press, Taylor & Francis Group, Boca Raton, 2011.
([5]) Cai, W.; Shalaev, V. M. *Optical Metamaterials: Fundamentals and Applications*, Springer: 2010.
([6]) Krishnamoorthy, H. N. S.; Jacob, Z; Narimanov, E.; Kretzschmar, I.; Menon, V. M. Metamaterial based broadband engineering of quantum dot spontaneous emission. **2009,** *arXiv:0912.2454*.
([7]) Noginov, M. A.; Li, H.; Barnakov,Y. A.; Dryden, D.; Nataraj, G.; Zhu, G., Bonner, C. E.; Mayy, M.; Jacob, Z.; Narimanov, E. E. Controlling spontaneous emission with metamaterials. *Opt. Lett.* **2010**, 35, 1863-1865.
([8]) Jacob, Z.; Kim, J.-Y.; Naik, G. V.; Boltasseva, A.; Narimanov, E. E.; Shalaev, V. M. Engineering photonic density of states using metamaterials. *Applied Physics B* ***2010***, 100, 215–218.
([9]) Tumkur, T.; Zhu, G.; Black, P.; Barnakov, Y. A.; Bonner, C. E.; Noginov, M. A.; Control of spontaneous emission in a volume of functionalized hyperbolic metamaterial. Appl. Phys. Lett. **2011**, 99, 151115.
([10]) Jacob, Z.; Smolyaninov, I. I.; Narimanov, E. E. Broadband Purcell effect: Radiative decay engineering with metamaterials. Appl. Phys. Lett. **2012**, 100, 181105.
([11]) Krishnamoorthy, H. N. S.; Jacob, Z.; Narimanov, E.; Kretzschmar, I.; Menon, V. M. Topological Transitions in Metamaterials. Science. **2012**, 336, 205-209.
([12]) Poddubny, A. N.; Belov, P. A.; Kivshar, Y. S. Spontaneous radiation of a finite-size dipole emitter in hyperbolic media. *Phys. Rev. A*. **2011**, 84, 023807.
([13]) Galfsky, T.; Krishnamoorty, H. N. S.; Newman, W.; Narimanov, E. E.; Jacob, Z.; Menon, V. M. Active hyperbolic metamaterials: enhanced spontaneous emission and light extraction. *Optica*. **2015**, 2, 62-65.
([14]) Lu, D.; Kan, J. J.; Fullerton, E. E.; Liu, Z. Enhancing spontaneous emission rates of molecules using nanopatterned multilayer hyperbolic metamaterials. *Nature Nanotechnology*. **2014**, 9, 48–53.
([15]) Gu, L.; Tumkur, T. U.; Zhu, G.; Noginov, M. A. Blue shift of spontaneous emission in hyperbolic metamaterial. *Scientific Reports*. **2014**, 4, 4969.

([16]) Gu, L.; Livenere, J. E.; Zhu, G.; Tumkur, T. U.; Hu, H.; Cortes, C. L.; Jacob, Z.; Prokes, S. M.; Noginov, M. A. Angular distribution of emission from hyperbolic metamaterials. *Scientific Reports*. **2014**, 4, 7327.
([17]) Andrew, P.; Barnes, W. L. Förster Energy Transfer in an Optical Microcavity. *Science.* **2000**, 290, 785-788.
([18]) Blum, C.; N. Zijlstra, N.; Lagendijk, A., Wubs, M.; Mosk, A. P.; Subramaniam, V.; Vos, W. L. Nanophotonic control of the Förster resonance energy transfer efficiency. *Phys. Rev. Let.* **2012**, 109, 203601.
([19]) Tumkur, T.; Kitur, J.; Bonner, C.; Poddubny, A.; Narimanov, E.; Noginov, M. Control of Förster energy transfer in vicinity of metallic surfaces and hyperbolic metamaterials. *Faraday Discussions*. **2015**, 178, 395-412.
([20]) Rodriguez, A. W.; Capasso, F.; Johnson, S. G. The Casimir effect in microstructured geometries. *Nature Photonics.* **2011**, 5, 211-221.
([21]) Noginov, M. A.; Barnakov, Y. A.; Liberman, V.; Prayakarao, S.; Bonner, C. E.; Narimanov, E. E. Long-range wetting transparency on top of layered metal-dielectric substrates. *Scientific Reports*. **2016**, 6, 27834.
([22]) Schwartz, T.; Hutchison, J. A.; Genet, C.; Ebbesen, T. W. Reversible Switching of Ultrastrong Light-Molecule Coupling, *Phys. Rev. Lett.* **2011**, 106, 196405.
([23]) Hutchison, J. A.; Schwartz, T.; Genet, C.; Devaux, E.; Ebbesen, T. W. Modifying Chemical Landscapes by Coupling to Vacuum Fields. *Angew. Chem. Int. Ed*. **2012**, 51, 1592 –1596.
([24]) Peters, V. N.; Tumkur, T. U.; Zhu, G.; Noginov, M. A. Control of a chemical reaction (photodegradation of the P3HT polymer) with nonlocal dielectric environments. Scientific Reports. **2015**, 5, 14620.
([25]) Peters, V. N.; Faruk, Md O.; Asane, J.; Alexander, R., Peters, D. A.; Prayakarao, S., Rout, S.; Noginov. Effect of Strong Coupling on Photodegradation of the Semiconducting Polymer P3HT". *Optica*. 2**019**, 6, 318-325.
([26]) Lee, K. J.; Xiao, Y.; Woo, J. H.; Kim, E.; Kreher, D.; Attias, A.-J.; Mathevet, F.; Ribierre, J.-C.; Wu, J. W.; André, P. Charge-transfer dynamics and nonlocal dielectric permittivity tuned with metamaterial structures as solvent analogues. *Nature Materials*. **2017**, 16, 722–729..
([27]) Kroemer, H. *Quantum Mechanics For Engineering: Materials Science and Applied Physics*; Prentice Hall, Inc.:1994.
([28]) Pantell, R. H.; Puthoff, H. E.. *Fundamentals of Quantum Electronics*; John Wyley & Sons, Inc: New York, London, Sydney, Toronto,1969..
([29]) Purcell, E. M. Spontaneous emission probabilities at radio frequencies. *Phys. Rev.* **1946**, 69, 681.
([30]) Drexhage, K. H. "Influence of a dielectric interface on fluorescence decay line", *Journal of Luminescence*. **1970**, 1,2, 693-701..
([31]) Drexhage, K. H. *Interaction of light with monatomic dye layers*; .in Progress in Optics, Volume XII, Emil Wolf, editor, North-Holland/American Elsevier, North Holland Publishing Company:, Amsterdam, London, pp. 164-234, 1974.
([32]) Vahala, K. J. Optical microcavities. *Nature*. **2003**, 424, 839–846.
([33]) Robinson, J. T.; Manolatou, C.; Chen, L.; Lipson, M. Ultrasmall Mode Volumes in Dielectric Optical Microcavities. 2005, *Phys. Rev. Lett.* **2005**, 95, 143901.
([34]) Painter, O.; Lee, R. K.; Scherer, A.; Yariv, A.; O'Brien, J. D.; Dapkus, P. D.; Kim, I. Two-Dimensional Photonic Band-Gap Defect Mode Laser. *Science*. **1999**, 284, 1819-1821.
([35]) Painter, O.; Vučković, J.; Scherer, A. Defect modes of a two-dimensional photonic crystal in an optically thin dielectric slab. *JOSA B*. **1999**, 16, 275-285.
([36]) Noda, S.; Fujita, M.; Asano, T. Spontaneous-emission control by photonic crystals and nanocavities. *Nature Photonics*. **2007**, 1, 449–458.
([37]) Joannopoulos, J. D.; Villeneuve, P. R.; Fan, S. Photonic crystals: putting a new twist on light. *Nature*. **1997**, 386, 143–149.
([38]) Catchpole, K. R.; Polman, A. Plasmonic solar cells. *Optics Express*. **2008**, 16, 21793-21800.
([39]) Viarbitskaya, S.; Teulle, A.; Marty, R.; Sharma, J.; Girard, C.; Arbouet, A.; Dujardin, E. Tailoring and imaging the plasmonic local density of states in crystalline nanoprisms. *Nature Materials.* **2013**, 12, 426–432.

([40]) Carminati, R.; Cazé, A.; Cao, D.; Peragut, F.; Krachmalnicoff V.;, Pierrat, R.;. De Wilde, Y. Electromagnetic density of states in complex plasmonic systems. *Surface Science Reports*. **2015**, 70, 1-41.
([41]) Belov, P. A.; Marqués, R.; Maslovski, S. I.; Nefedov, I. S.; Silveirinha, M.; Simovski, C. R.; Tretyakov S. A. Strong spatial dispersion in wire media in the very large wavelength limit. *Phys. Rev. B*. **2003**, 67, 113103.
([42]) Smith, D. R.; Schurig, D. Electromagnetic wave propagation in media with indefinite permittivity and permeability tensors. *Phys. Rev. Lett.* **2003,** 90, 077405.
([43]) Jacob, Z.; Alekseyev, L. V.; Narimanov, E. E. Optical Hyperlens: Far-field imaging beyond the diffraction limit beyond the diffraction limit. *Opt. Express*. **2006**, 14, 8247–8256.
([44]) Salandrino, A.; Engheta, N. Far-field subdiffraction optical microscopy using metamaterial crystals: Theory and simulations. *Phys. Rev. B*. **2006**, 74, 075103.
([45]) Yao, J.; Liu, Z.; Liu, Y.; Wang, Y.; Sun, C.; Bartal, G.; Stacy, A. M.; Zhang, X. Optical negative refraction in bulk metamaterials of nanowires. *Science*. **2008**, 321, 930.
([46]) Poddubny, A.; Iorsh, I.; Belov, P.; Kivshar, Y. Hyperbolic metamaterials. *Nature Photonics*. **2013**, 7, 948–957.
([47]) Shekhar, P.; Atkinson, J.; Jacob, Z. Hyperbolic metamaterials: fundamentals and applications. *Nano Convergence.* **2014,** 1, 14.
([48]) Podolskiy, V. A.; Ginzburg, P.; Wells, B.; Zayats, A. V. Light emission in nonlocal plasmonic metamaterials. Faraday Discussions. **2015**, 178, 61.
([49]) Valeur, B.; Berberan-Santos, M. N. *Molecular fluorescence: principles and applications*; John Wiley & Sons, 2012.
([50]) Bachmann, V.; Ronda, C.; Meijerink, A. Temperature Quenching of Yellow Ce^{3+} Luminescence in YAG:Ce. Chem. Mater. **2009**, 21, 2077–2084.
([51]) Anger, P.; Bharadwaj, P.; L. Novotny. Enhancement and Quenching of Single-Molecule Fluorescence. *Phys. Rev. Lett*. **2006**, 96, 113002.
([52]) Noginov, M. A.; Zhu, G.; Belgrave, A. M.; Bakker, R.; Shalaev, V. M.; Narimanov, E. E.; Stout, S.; Herz, E.; Suteewong, T.; Wiesner, U.; Demonstration of a spaser-based nanolaser. *Nature*. 2009, 460, 1110-1112.
([53]) Kéna-Cohen, S.; Forrest, S. R. Room-temperature polariton lasing in an organic single-crystal microcavity. *Nature Photonics*. **2010**, 4, 371–375.
[54] Agranovich, V. M., Galanin, M. D. *Electronic Excitation Energy Transfer in Condenced Matter*; North-Holland Publishing Company: Amsterdam, New York, Oxford, 1982.
([55]) Förster, T. Zwischenmolekulare Energiewanderung und Fluoreszenz. *Annalen der Physik*, **1948**, 437, 55-75.
([56]) Förster, T. Experimentelle und theoretische Untersuchung des zwischenmolekularen Übergangs von Elektronenanregungsenergie. *Zeitscrift fur Naturforshung*. **1949**, 4a, 321-327.
([57]) Förster, T. 10th Spiers Memorial Lecture. Transfer mechanics of Electronic Excitation; Discussions of the Faraday Society. **1959**, 27, 7-17.
([58]) Van der Waals, J. D. Over de Continuiteit van den Gas- en Vloeistoftoestand (on the continuity of the gas and liquid state)", doctoral thesis; Sijthoff, A. W.,1873.
([59]) Keesom, W. H. The second viral coefficient for rigid spherical molecules, whose mutual attraction is equivalent to that of a quadruplet placed at their centre. *Proc. R. Acad. Sci*. **1915**, 18, 636-646.
([60]) Keesom, W. H. The quadrupole moments of the oxygen and nitrogen molecules. *Proc. K. Ned. Akad. Wet*. **1920**, 23, 939-942.
([61]) Keesom, W. H. Van der Waals attractive force. *Physikalische Zeitschrift*. **1921**, 22, 129–141.
([62]) Debye, P. Van der Waals cohesion forces. *Physikalische Zeitschrift*. **1920**, 21, 178-187.
([63]) Debye, P. Molecular forces and their electrical interpretation. *Physikalische Zeitschrift*. **1921**, 22, 302-308.
([64]) London, F. Zur Theorie und Systematik der Molekularkräfte. *Zeitschrift für Physik*. **1930**, 63, 245-279.
([65]) Van Oss, C. J.; Chaudhury, M. J.; Good, R. J. Interfacial Lifshits-van der Waals and polar interactions in macroscopic systems. *Chem. Rev.* **1988**, 88, 927-41.
([66]) Lifshits, E. M. The theory of molecular attractive forces between solids. Soviet Physics JETP. 1956, 2, 73-83.

[67]) Dzyaloshinski, I. E.; Lifshitz, E. M.; Pitaevskii, L. P. The general theory of van der Waans forces. *Advan. Phys.* **1961**, 10, 165.
([68]) Mahanthy, J. B.; Ninham, W. *Dispersion Forces*; Academic Press: London,1976.
([69]) Israelachvili, J. N. *Intermolecular and Surface Forces*, Third edition; Academic Press (imprint of Elsevier): Amsterdam, 2011.
([70]) Casimir, H. B. G. On the attraction between two perfectly conducting plates. *Proc. K. Ned. Akad. Wet.* **1948**, 51, 793–795.
([71]) Casimir, H. B. G.; Polder, D. The influence of retardation on the London-van der Waals forces. *Phys. Rev.* **1948**, 73, 360-372.
([72]) Hamaker, H. C. The London–van der Waals Attraction between Spherical Particles. *Physica*. **1937**, 4, 1058–72.
([73]) French, R. H. Origins and Applications of London Dispersion Forces and Hamaker Constants in Ceramics. *J. Am. Ceram. Soc.* **2000**, 83, 2117–46.
([74]) Khitrova, G.; Gibbs, H. M.; Kira, M.; Koch, S.; Scherer, A. Vacuum Rabi splitting in semiconductors. *Nature Physics.* **2006**, 2, 81-90 (2006).
([75]) Törmä, P.; Barnes, W. Strong Coupling between Surface Plasmon Polaritons and Emitters: A Review, *Rep. Prog. Phys.* **2015** 78, 013901.
([76]) Ebbesen, T. W. Hybrid Light-Matter States in a Molecular and Material Science Perspective. *Acc. Chem. Res*. **2016**, 49, 2403-2412.
([77]) i Morral, A. F.; Stellacci, F.; Ultrastrong routs to new chemistry. *Nature Materials*. **2012** 11, 272-273.
([78]) Jahnke,F.; Kira, M.; Koch, S. W.; Khitrova, G.; Lindmark, E. K.; Nelson, Jr. T. R.; Wick, D. V.; Berger, J. D.; Lyngnes, O.; Gibbs, H. M.; Tai, K. Excitonic Nonlinearities of Semiconductor Microcavities in the Nonperturbative Regime. *Phys. Rev. Lett.* **1996**, 77, 5257-5260 .
([79]) Bellessa, J.; Bonnand, C.; Plenet, J.; Mugnier, J.; Strong Coupling between Surface Plasmons and Excitons in an Organic Semiconductor, *Phys. Rev. Lett*. **2004**, 93, 036404.
([80]) Kéna-Cohen, S.; Maier, S. A., Bradley, D. D. C. “ltrastrongly Coupled Exciton-Polaritons in Metal-Clad Organic Semiconductor Microcavities. *Adv. Opt. Mater*. **2013**, 1, 827-833.
([81]) Gambino, S.; Mazzeo, M.; Genco, A.; Di Stefano, O.;, Savasta, S.; Patanè, S.; Ballarini, D.; Mangione, F.; Lerario, G.; Sanvitto, D.; Gigli, G. Exploring Light-Matter Interaction Phenomena under Ultrastrong Coupling Regime. *ACS Photonics*. **2014**, 1, 1042-1048.
([82]) Marcus, R. A. On the theory of oxidation-reduction reactions involving electron transfer I. *J. Chem. Phys*. **1956**, 24, 966-978.
([83]) Marcus, R. A. Electrostatic free energy and other properties of states having nonequilibrium polarization I. *J. Chem. Phys*. **1956**, 24, 979-989.
([84]) Marcus, R. A. Electron transfer reactions in chemistry. Theory and experiment. *Rev. Mod. Phys*. **1993** 65, 599-610.
([85]) Marucs, R. A.; Sutin, N. Electron transfers in chemistry and biology. Biochimica et Biophysica Acta. 1985, 811, 265-322.
([86]) Parada, G. A.; Goldsmith, Z. K.; Kolmar, S.; Rimgard, B. P.; Mercado, B. Q.; Hammarström, L.; Hammes-Schiffer, S.; Mayer, J. M. Concerted proton-electron transfer reactions in the Marcus inverted region, *Science*. 2019, 364, 471-475.
([87]) Sein, L. T.; Weib, Y.; Jansena, S. A. Corrosion inhibition by aniline oligomers through charge transfer: a DFT approach. *Synthetic Metals*. **2004**, 143, 1–12.
([88]) Marcus, R. A. On the theory of chemiluminescent electron-transfer reactions. *J. Chem. Phys.* **1965**, 43, 2654 - 2657.
([89]) Adams, D. M.; Brus, L.; Chidsey, C. E. D.; Creager, S.; Creutz, C.; Kagan, C. R.; Kamat, P. V.; Lieberman, M.; Lindsay, S.; Marcus, R. A.; Metzger, R. M.; Michel-Beyerle, M. E.; Miller, J. R.; Newton, M. D.; Rolison, D. R.; Sankey, O.; Schanze, K. S.; Yardley, J.; and X. Zhu, Charge transfer on the nanoscale: current status. *J. Phys. Chem B*. **2003**, 107, 6668-6697.
([90]) Kim, J.; Drachev, V. P.; Jacob, Z.; Naik, G. V.; Boltasseva, A.; Narimanov, E. E.; Shalaev, V. M. Improving the radiative decay rate for dye molecules with hyperbolic metamaterials, *Optics Express*. **2012**, 20, 8100-8116.
([91]) Bogdanov, S.; Shalaginov, M. Y.; Boltasseva, A.; Shalaev, V. M. Material platforms for integrated quantum photonics. *Opt. Mater. Express*. **2017**, 7, 111-132.

([92]) Sudarkin, A. N.; Demkovich, P. A. Excitation of surface electromagnetic waves on the boundary of a metal with an amplifying medium. *Sov. Phys. Tech. Phys*. 1989, 34, 764–766.
([93]) Seidel, J.; Grafstroem, S.; Eng, L. Stimulated emission of surface plasmons at the interface between a silver film and an optically pumped dye solution. *Phys. Rev. Lett.* **2005**, 94, 177401.
([94]) Noginov, M. A.; Zhu, G.; Mayy, M.; Ritzo, B. A.; Noginova, N.; Podolskiy, V. A. Stimulated emission of surface plasmon polaritons. *Phys. Rev. Lett*. **2008**, 101, 226806.
([95]) Kitur, J. K.; Zhu, G.; Noginov, M. A.; Low-threshold stimulated emission of surface plasmons polaritons. *J. Opt.* **2014**,16, 114020.
([96]) Kitur, J. K.; Gu, L.; Tumkur, T.; Bonner, C.; Noginov, M. A. Stimulated emission of surface plasmons on top of metamaterials with hyperbolic dispersion. *ACS Photonics*. **2015**, 2, 1019-1024.
([97]) Dung, H. T.; Knöll, L.; Welsch, D. G.; Three-dimensional quantization of the electromagnetic field in dispersive and absorbing inhomogeneous dielectrics. *Phys. Rev. A*. **1998**, 57, 3931.
([98]) Nakamura, T.; Fujii, M.; Imakita, K,; Hayashi, S. Modification of energy transfer from Si nanocrystals to Er^{3+} near a Au thin film. *Phys. Rev. B.* **2005**, 72, 235412.
([99]) Nakamura, T.; Fujii, M.; Miura, S.; Inui, M.; Hayashi, S. Enhancement and suppression of energy transfer from Si nanocrystals to Er ions through a control of the photonic mode density, *Phys. Rev. B*. **2006**, 74, 045302.
([100]) Sun, Q. C.; Mundoor, H.; Ribot, J. C.; Singh, V.; Smalyukh, I. I.; Nagpal, P. Plasmon-enhanced energy transfer for improved upconversion of infrared radiation in doped-lanthanide nanocrystals. *Nano Lett*. **2013**, 14, 101-106 (2013).
([101]) de Dood, M.; Knoester, J., Tip, A.; Polman, A. Förster transfer and the local optical density of states in erbium-doped silica. 2005 Phys. Rev. B 71, 115102.
([102]) Schleifenbaum, F.; Kern, A. M.; Konrad, A.; Meixner, A. J. Dynamic control of Förster energy transfer in a photonic environment. *Phys. Chem. Chem. Phys.* **2014**, 16, 12812-12817.
([103]) Rabouw, F. T.; den Hartog, S. A.; Senden, T.; Meijerink, A. Photonic effects on the Förster resonance energy transfer efficiency. *Nature Commun*. **2014**, 5, 3610.
([104]) Kim, K.-S.; Kim, J.-H.; Kim, H.; Laquai, F.; Arifin, E.; Lee, J.-K.; Yoo, S.I.; Sohn, B.-H. Switching off FRET in the hybrid assemblies of diblock copolymer micelles, quantum dots, and dyes by plasmonic nanoparticles. *ACS Nano*. **2012**, 6, 5051–5059.
([105]) Prayakarao, S.; Koutsares, S.; Bonner, C. E.; Noginov, M. A. Inhibition of the Concentration Quenching of HITC Dye in Nonlocal Plasmonic Environments. *Conference on Lasers and Electro-Optics, OSA Terchnical Digest (online) (Optical Society of America, 2018),* paper FW4G.6.
([106]) Prayakarao, S.; Koutsares, S. R.; Bonner, C. E.; Noginov, M. A. Effect of Nonlocal Metal-Dielectric Environments on Concentration Quenching of HITC dye. *JOSA B* (submitted).
([107]) Chance, R. R.; Prock, A.; Silbey, R. Frequency shifts of an electric-dipole transition near a partially ref1ecting surface. *Phys. Rev. B.* **1975**, 12, 1448 – 1452.
([108]) Li, Y.; Pham, J. Q.; Johnston, K. P.; Green, P. F. Contact Angle of Water on Polystyrene Thin Films: Effects of CO Environment and Film Thickness. *Langmuir*. **2007**, 23, 9785–9793.
([109]) Roncali, J. Conjugated poly(thiophenes): synthesis, functionalization, and applications. *Chem. Rev*. **1992**, 92, 1711-1738.
([110]) Hintz, H.; Egelhaaf, H.-J.; Lüer, L.; Hauch, J.; Peisert, H.; Chassé, T. Photodegradation of P3HT - a systemic study of environmental factors. *Chemistry of Materials.* **2011**, 23, 145-154.
([111]) Hintz, H.; Sessler, C.; Peisert, H.; Egelhaaf, H.-J.; Chassé, T. "Wavelength-dependent pathways of Poly-3-hexylthiophene photo-oxidation. *Chemistry of Materials*. **2012**, 24, 2739-2743.
([112]) Tian, W. J.; Zhang, H. Y.; Shen, J. C. Some properties of interfaces between metals and polymers. *Surface Review and Letters*. **1997**, 4, 703-708.
([113]) Bond, G. C. Homogeneous and heterogeneous catalysis by noble metals; in *Homogeneous Catalysis,* 25-34, Luberoff, B. J. Ed., Johnson, Matthey and Co. Ltd.
([114]) Wang, P.; Huang, P., B.; Dai, Y.; Whangbo, M.-H.; Plasmonic photocatalysts: harvesting visible light with noble metal nanoparticles. *Phys. Chem. Chem. Phys.* **2012**, 14, 9813-9825.
([115]) Peters, V. N.; Alexander, R.; Peters, D. A.; Noginov, M. A. Study of the effect of excited state concentration on photodegradation of the P3HT polymer. *Scientific Reports.* **2016**, 6, 33238 .
([116]) Smith, D. Y.; Shiles, E.; Inokuti, M.; The optical properties of metallic aluminum. i*Handbook of Optical Constants of Solids*, 369-406, Palik, E. D., Ed.; Academic Press: Burlington, 1997.

([117]) Johnson, P. B.; Christy, R. W.; Optical constants of the noble metals. *Phys. Rev. B*. **1972**, 6, 4370-4379.
([118]) Peters, V. N.; Yang, C.; Prayakarao, S.; Noginov, M. A. Effect of metal–dielectric substrates on chemiluminescence kinetics. *Journal of the Optical Society of America B*. **2019**, 36, E132-E138.
([119]) Rauhut, M. M.; Chemiluminescence from concerted peroxide decomposition reactions. *Accounts of Chemical Research.* **1969**, 2, 80-87.
([120]) Schuster, G. B. Chemiluminescence of organic peroxides. Conversion of ground-state reactants to excited-state products by the chemically initiated electron-exchange luminescence mechanism. *Accounts of Chemical Research.* **1979**, 12, 366-373.
([121]) Hutchison, J. A.; Liscio, A.; Schwartz, T.; Canaguier-Durand, A.; Genet, C.; Palermo, V.; Samorì, P.; Ebbesen, T. W. Tuning the Work-Function via Strong Coupling. *Adv. Mater*. **2013**, 25, 2481-2485.
([122]) Orgiu, E.; George, J.; Hutchison, J. A.; Devaux, E.; Dayen, J. F.; Doudin, B.; Stellacci, F.; Genet, C.; Schachenmayer, J.; Genes, C.; Pupillo, G.; Samorì, P.; Ebbesen, T. W. Conductivity in organic semiconductors hybridized with the vacuum field. *Nature Materials*. **2015**, 14, 1123-1129.
([123]) Gonzalez-Ballestero, C.; Feist, J.; Moreno, E.; Garcia-Vidal, F. J. Harvesting Excitons through Plasmonic Strong Coupling. *Phys. Rev. B.* **2015**, 92, 121402.
([124]) Schachenmayer, J.; Genes, C.; Tignone, E.; Pupillo, G. Cavity enhanced transport of excitons. *Phys. Rev. Lett.* **2015**, 114, 196403.
([125]) Garcia-Vidal, F. J.; Pendry, J. B. Collective Theory for Surface Enhanced Raman Scattering. *Phys*. *Rev. Lett.* **1996**, 77, 1163.
([126]) del Pino, J.; Feist, J.; Garcia-Vidal, F. J. Signatures of Vibrational Strong Coupling in Raman Scattering. *J. Phys. Chem. C*. **2015,** 119, 29132-29137.
([127]) Shalabney, A.; George, J.; Hiura, H.; Hutchison, J. A.; Genet, C.; Hellwig, P.; Ebbesen, T. W. Enhanced Raman Scattering from Vibro-Polariton Hybrid States. *Angewandte Chemie*. 2015, 54, 7971-7975.
([128]) Zhong, X.; Chervy, T.; Zhang, L.; Thomas, A.; George, J.; C. Genet, Hutchison, J. A.; Ebbesen, T. W. Energy transfer between spatially separated entangled molecules; *Angew. Chem. Int. Ed*. **2017**, 56, 9034 –9038.
([129]) TDBC: 5,5′,6,6′-tetrachloro- di-(4-sulfobutyl) benzimidazolocarbocyanine.
([130]) Munkhbat, B.; Wersäll, M.; Baranov, D. G.; Antosiewicz, T. J.; Shegai, T. Suppression of photo-oxidation of organic chromophores by strong coupling to plasmonic nanoantennas. *Sci. Adv.*, **2018**, eaas9552.
([131]) Galego, J.; Garcia-Vidal, F. J.; Feist, J. Suppressing photochemical reactions with quantized light fields, *Nature Comm*. **2016**, 8, 13841.
([132]) Kowalewski, M.; Bennett, K.; Mukamel, S. Cavity Femtochemistry: manipulating nonadiabatic dynamics at avoided crossings. *J. Phys. Chem. Lett*. **2016**, 7, 2050−2054.
([133]) Galego,J.; Garcia-Vidal, F. J.; Feist, J.; Many-molecule reaction triggered by a single photon in polaritonic chemistry. *Phys. Rev. Lett*. **2016**, 119, 136001.
([134]) Herrera, F.; Spano, F. C. Cavity-Controlled Chemistry in Molecular Ensembles. *Phys. Rev. Lett*. **2016**, 116, 238301.
([135]) Dunkelberger, A. D.; Spann, B. T.; Fears, K. P.; Simpkins, B. S.; Owrutsky, J. C. Modified relaxation dynamics and coherent energy exchange in coupled vibration-cavity polaritons. *Nature Comm.* **2016**, 7, 13504.
([136]) Simpkins, B. S.; Fears, K. P.; Dressick, W. J.; Spann, B. T.; Dunkelberger, A. D.; Owrutsky, J. C. Spanning strong to weak normal mode coupling between vibrational and Fabry−Perot cavity modes through tuning of vibrational absorption strength. *ACS Photonics*. **2015**, 2, 1460−1467.
([137]) Thomas, A.; George, J.; Shalabney, A.; Dryzhakov, M.; Varma, S.; Moran, J.; Chervy, T.; Zhong, X.; Devaux, E.; Genet, C.; Hutchison, J.; Ebbesen, T. W. Ground-state chemical reactivity under vibrational coupling to the vacuum electromagnetic field. *Angewandte Chemie*. **201**6, 55, 11462-11466.
([138]) Ribeiro, R. F.; Martínez-Martínez, L. A.; Du, M.; Campos-Gonzalez-Anguloa, J.; Yuen-Zhou, J. Polariton chemistry: controlling molecular dynamics with optical cavities. *Chem. Sci.* **2018**, 9, 6325-6339.
([139]) Stranius, K.; Hertzog, M.; Börjesson, K.; Selective manipulation of electronically excited states through strong light–matter interactions. Nature Comm. 2018, 9, 2273.

[140] Aslam, U.; Rao, V. G.; Chavez, S.; Linic, S. Catalytic Conversion of Solar to Chemical Energy on Plasmonic Metal Nanostructures. *Nat. Catal.* **2018**, 656−665.

[141] Zhan, C.; Chen, X.-J.; Yi, J.; Li, J.-F.; Wu, D.-Y.; Tian, Z.-Q. From Plasmon-Enhanced Molecular Spectroscopy to Plasmon- Mediated Chemical Reactions. *Nat. Rev. Chem*. **2018**, 216−230.

[142] Christopher, P.; Xin, H.; Linic, S. Visible-Light-Enhanced Catalytic Oxidation Reactions on Plasmonic Silver Nanostructures. *Nat. Chem.* **2011**, 467−472.

[143] Gargiulo, J.; Berte,́ R.; Li, Y.; Maier, S. A.; Corteś, E. From Optical to Chemical Hot Spots in Plasmonics. A*cc. Chem. Res*. **2019**.

[144] Brongersma, M. L.; Halas, N. J.; Nordlander, P. Plasmon-Induced Hot Carrier Science and Technology. *Nat. Nanotechnol*. **2015**, 25−34.

[145] Zhang, Y.; He, S.; Guo, W.; Hu, Y.; Huang, J.; Mulcahy, J. R.; Wei, W. D. Surface-Plasmon-Driven Hot Electron Photochemistry. *Chem. Rev*. **2018**, 2927−2954.

[146] Schneider, C.; Rahimi-Iman, A.; Kim, N. Y.; Fischer, J.; Savenko, I. G.; Amthor, M. ; Lermer, M.; Wolf, A.; Worschech, L.; Kulakovskii, V. D.; Shelykh, I. A.; Kamp, M.; Reitzenstein, S.; Forchel, A.; Yamamoto, Y.; Höfling, S. An electrically pumped polariton laser. *Nature*. **2013**, 497, 348-352.

[147] Plumhof, J. D.; Stöferle, J. D.; Mai, L.; Scherf, U.; Mahrt, R. F. Room-temperature Bose–Einstein condensation of cavity exciton–polaritons in a polymer. Nature Materials. **2014**, 13, 247- 252.

[148] Daskalakis, K. S.; Maier, S. A.; Murray, R.; Kéna-Cohen, S. Nonlinear interactions in an organic polariton condensate. *Nature Materials*. **2014**, 13, 271-278.

[149] Paschos, G. G.; Somaschi, N.; Tsintzos, S. I.; Coles, D.; Bricks, J. L.; Hatzopoulos, Z.; Lidzey, D. G.; Lagoudakis, P. G.; Savvidis, P. G. Hybrid organic-inorganic polariton laser. *Scientific Reports*. **2017**, 7, 11377.